

# The Luminosity Profiles of Brightest Cluster Galaxies

C.J. Donzelli, H. Muriel

*IATE, Observatorio Astronómico OAC, Laprida 854, X5000BGR, Córdoba, Argentina*  
*Consejo Nacional de Investigaciones Científicas y Técnicas (CONICET), Avenida Rivadavia 1917,*  
*C1033AAJ, Buenos Aires, Argentina*

J. P. Madrid

*Centre for Astrophysics and Supercomputing, Swinburne University of Technology, Hawthorn, VIC 3122,*  
*Australia*

## ABSTRACT

We have derived detailed R band luminosity profiles and structural parameters for a total of 430 brightest cluster galaxies (BCGs), down to a limiting surface brightness of  $24.5 \text{ mag arcsec}^{-2}$ . Light profiles were initially fitted with a Sérsic's  $R^{1/n}$  model, but we found that 205 ( $\sim 48\%$ ) BCGs require a double component model to accurately match their light profiles. The best fit for these 205 galaxies is an inner Sérsic model, with indices  $n \sim 1 - 7$ , plus an outer exponential component.

Thus, we establish the existence of two categories of the BCGs luminosity profiles: *single* and *double* component profiles. We found that double profile BCGs are brighter ( $\sim 0.2 \text{ mag}$ ) than single profile BCG. In fact, the Kolmogorov-Smirnov test applied to these subsamples indicates that they have different total magnitude distributions, with mean values  $M_R = -23.8 \pm 0.6 \text{ mag}$  for single profile BCGs and  $M_R = -24.0 \pm 0.5 \text{ mag}$  for double profile BCGs. We find that partial luminosities for both subsamples are indistinguishable up to  $r = 15 \text{ kpc}$ , while for  $r > 20 \text{ kpc}$  the luminosities we obtain are on average  $0.2 \text{ mag}$  brighter for double profile BCGs. This result indicates that extra-light for double profile BCGs does not come from the inner region but from the outer regions of these galaxies.

The best fit slope of the Kormendy relation for the whole sample is  $a = 3.13 \pm 0.04$ . However, when fitted separately, single and double profile BCGs show different slopes:  $a_{\text{single}} = 3.29 \pm 0.06$  and  $a_{\text{double}} = 2.79 \pm 0.08$ . Also, the logarithmic slope of the metric luminosity  $\alpha$  is higher in double profile BCGs ( $\alpha_{\text{double}} = 0.65 \pm 0.12$ ) than in single profile BCGs ( $\alpha_{\text{single}} = 0.59 \pm 0.14$ ). The mean isophote outer ellipticity (calculated at  $\mu \sim 24 \text{ mag arcsec}^{-2}$ ) is higher in double profile BCGs ( $e_{\text{double}} = 0.30 \pm 0.10$ ) than in single profile BCGs ( $e_{\text{single}} = 0.26 \pm 0.11$ ). Similarly, the mean absolute value of inner minus outer ellipticity is also higher in double profile BCGs.

On the other hand, we did not find differences between these two BCGs categories when we compared global cluster properties such as the BCG-projected position relative to the cluster X-ray center emission, X-ray luminosity, or BCG orientation with respect to the cluster position angle.

*Subject headings:* galaxies: clusters: general — galaxies: elliptical and lenticular

## 1. Introduction

Brightest cluster galaxies (BCGs) are the most massive and most luminous galaxies in the uni-

verse today. BCGs are so massive ( $M_{\text{star}} > 10^{11} M_{\odot}$ ) that their formation and evolution is closely tied to the large scale structure of the universe (Conroy et al. 2007). Semi-analytical mod-

els show how BCGs are formed through complex hierarchical merging of many small galaxies and originate within the densest dark matter halos of primordial density fluctuations. BCGs reside only in overdense regions of the Universe such as galaxy clusters and groups where merging occurs at a high rate over cosmic time (de Lucia & Blaizot 2007). It is precisely the accretion of numerous stellar systems that give the BCGs their apparently homogeneous properties. For instance, their total luminosities are relatively constant and can be used as standard candles (Lauer & Postman 1992).

For several decades the luminosity profiles of elliptical galaxies were modeled with the empirical  $R^{1/4}$  de Vaucouleurs law (de Vaucouleurs 1948). However Lugger (1984) and Schombert (1986) showed that most elliptical galaxies have a flux excess at large radii with respect to the  $R^{1/4}$  model. Schombert (1987) modelled the BCG light profiles with a power law rather than the de Vaucouleurs law underscoring the different nature of BCGs and standard elliptical galaxies.

A model used virtually by every author in recent years to fit the light profiles of a wide range of stellar systems is the generalization of the de Vaucouleurs law introduced by Sérsic (1963, 1968). The Sérsic model in the form  $R^{1/n}$  is a mixture of bulge and disk components using only three free parameters ( $\mu_e$ ,  $r_e$ , and  $n_s$ ) instead of four ( $\mu_e$ ,  $r_e$ ,  $\mu_0$ , and  $r_0$ ) (see Section 3 and the comprehensive review of Graham and Driver 2005).

More recently, several papers have suggested that a simple Sérsic  $R^{1/n}$  law does not properly model the luminosity profile of some elliptical (usually cD) galaxies. Gonzalez et al. (2003, 2005) found that the best fit to the light profiles of 30 BCGs was a double  $R^{1/4}$  de Vaucouleurs profile. Seigar et al. (2007) studied the light profiles of five cD galaxies and showed that a Sérsic plus an exponential function are necessary to accurately reproduce an inner and an outer component present in their surface brightness profiles. Donzelli et al. (2007) estimated that roughly half of 82 elliptical galaxies belonging to the 3CR radio catalog also require a Sérsic + exponential model to properly fit their light profiles. Using numerical simulations Hopkins et al. (2009) propose that dissipational mergers are at the origin of the double components light profiles in the core of elliptical galaxies. According to their models a violent re-

laxation of stars whose parent galaxies participate in the merger is responsible for the creation of an outer component while a central starburst gives rise to the inner component.

We use a homogeneous and uniquely large sample of ground-based imaging of Abell clusters to carefully examine the luminosity profiles of 430 BCGs and determine the best fitting function and structural parameters. This is key to properly constrain dynamical models and the merging history of these galaxies.

The paper is organized as follows. In Section 2, we present the observations and reductions, while in Section 3 we describe data processing. Light profile fitting procedure and structural parameters are discussed in Section 4, while in Section 5 we discuss the results and in Section 6 we summarize the conclusions.

## 2. Observations

BCG images used in this work were provided by M. Postman (STScI) who kindly gave us access to the raw data. They were obtained under photometric conditions using the KPNO 2.1 m and 4 m telescopes, and the CTIO 1.5 m telescope between 1989 November and 1995 April over a total of 13 observing runs (see Table 1). Five of these runs are described in more detail in Postman & Lauer (1995). Briefly, all the images were acquired in the Kron-Cousins  $R_c$  band and have typically exposure times of 200-600 s. During these runs seeing conditions were very good to fair, namely, FWHM =  $1''$ - $2''$ , and nights were photometric.

In order to flat field the images a series of dome flats were obtained each night. This allowed for flatfielding with a typical accuracy better than 0.5% of the sky level. Photometric calibration was obtained by observing 10-15 Landolt (1983) standard stars per night. This also enabled us to calculate extinction coefficients and to check the zero point on each night of the observing runs. The overall photometric accuracy was better than 0.02 mag, much smaller than the typical errors of the BCG photometric parameters, which are more sensitive to background subtraction, and fitting models.

One of the key points of this homogeneous sample is that approximately 50 BCGs were observed in common between the different runs. Many of

these BCGs were actually observed in five or more runs. This not only allowed us to verify and compare reductions for all observing runs, but also to improve the accuracy of the luminosity profiles as discussed in the next section. The rms scatter for the integrated magnitudes of the galaxies is 0.03 mag, while for the luminosity profiles at  $\mu_R = 22.5$  mag arcsec<sup>-2</sup> is 0.11 mag arcsec<sup>-2</sup>.

### 3. Data Processing and Sky Level

All images were processed following the standard recipes: bias and flat field corrections using IRAF routines. After this process we carefully inspect the images in order to determine the best method to subtract the sky background. Gauging the sky is a crucial step since sky subtraction has a significant influence on the faint end of the luminosity profiles and therefore on the structural parameters we derive. In most cases a two-dimensional first-degree polynomial was sufficient to give an accurate fit to the sky, and we used the residuals distribution to estimate the uncertainty of the sky level  $\sigma_{sky}$ . The importance of sky cleaning is summarized in detail in Coenda et al. (2005).

Similar tests were made to measure the effect of seeing on the luminosity profiles. The effects of seeing dictate that the minimum radius for a suitable fit to the luminosity profile is  $r = 1.5 \times \text{FWHM}$ , this is particularly true for large galaxies, i.e., apparent radius greater than  $\sim 12 \times \text{FWHM}$  (Coenda et al. 2005). We show in detail in the next section that BCG galaxies were relatively bright and extended and in most cases the apparent radius of the galaxy was greater than  $20''$ .

### 4. Luminosity Profiles and Profile Fitting

We use the ELLIPSE routine (Jedrzejewski, 1987) within Space Telescope Science Analysis System (STSDAS) to extract the luminosity profiles of the BCGs. We apply this routine to the processed, sky subtracted images. In many cases galaxy overlapping is an issue due to the crowded fields around BCGs. To solve this, we apply the technique described in Coenda et al. (2005) which consists in masking the overlapping regions before profile extraction. Then we obtain the luminosity profile and structural parameters (center co-

ordinates, ellipticity, and position angle of the isophotes), and construct a model BCG galaxy that is subtracted from the original image. The residual image is then used to extract the luminosity profile of the overlapping galaxies. The process is repeated several times until the profile of the target galaxy converges.

Isophote fitting was performed down to a count level of  $2\sigma_{sky}$ ; i.e., the fitting procedure was stopped when the isophote level was around twice the background dispersion (pixel-to-pixel variance), which in our case corresponds to surface magnitudes between  $\mu_R \sim 23.5 - 24.5$  mag arcsec<sup>-2</sup>, depending on the observational run when the cluster was observed.

For each cluster, we usually obtain the luminosity profiles for the three brightest galaxies in the field. This preliminary selection is made by eye. In those cases where the selection is not obvious, we also obtain additional luminosity profiles, i.e., for the five brightest galaxies. The final BCG selection is made through the galaxy metric luminosity, that is the luminosity enclosed in a radius of 14.5 kpc, we also included galaxy redshift to ensure cluster membership. Redshift data were obtained from the NASA/IPAC Extragalactic Database (NED).

As discussed in the introduction, there are a wide variety of functions to perform luminosity profile fitting. We adopted the Sérsic profile  $R^\beta$ , where the concentration parameter  $\beta = 1/n$  is the inverse of the Sérsic index (Sérsic 1968):

$$I(r) = I_e \exp\left\{-b_n \left[\left(\frac{r}{r_e}\right)^\beta - 1\right]\right\}. \quad (1)$$

In this equation  $I_e$  is the intensity at  $r = r_e$  the radius that encloses half of the total luminosity (also known as the effective radius or half-light radius). In this context  $b_n$  can be calculated using  $b_n \sim 2n - 0.33$  (Caon et al. 1993).

We use the NFIT1D routine within STSDAS to find the coefficients that best fit the light profiles of each galaxy. This task uses a  $\chi^2$  minimization scheme to fit the best non linear functions to the light profiles tables we obtained with ELLIPSE (Schombert & Bothun 1987). The fitting procedure is carried out only in the portion of the galaxy surface brightness profile where the signal-to-noise ratio was greater than 3 ( $S/N > 3$ ). We

did this in order to avoid the regions at the faint end of the luminosity profiles, in which errors are large. Moreover, we have also excluded the inner 3"-4" of the luminosity profiles to avoid the blurring effects of seeing (see the test described in Coenda et al. 2005).

Errors on the structural parameters were calculated following the method described by Coenda et al. (2005). Briefly, this technique consists of creating test images with model galaxies that have known luminosity profile parameters. Then we artificially add and subtract to those images a constant value corresponding to  $\sigma_{sky}$ . Finally we extract and refit the new luminosity profile as explained above. These newly obtained parameters give us the respective upper and lower limits.

To a first approximation a single Sérsic model provides a good fit to the light profile of our sample of BCGs, as shown by Graham et al. (1996). However, for almost half of the sample we noticed that a single Sérsic function fails to properly reproduce the BCGs surface brightness in the range  $\sim 22.0 \text{ mag arcsec}^{-2}$ . Note that this case is very similar to that presented in La Barbera et al. (2008, their Figure 18). It is evident that the Sérsic function do not properly fit the luminosity profiles of these elliptical galaxies in the inner 4'', where the residuals are almost  $\sim 0.3 \text{ mag arcsec}^{-2}$ .

It is not necessary to have very deep luminosity profiles, as in the case of Seigar et al. (2007), to realize that for certain galaxies, even in regions of bright surface luminosity, a single Sérsic model cannot account for the concave shape of the luminosity profile.

For these galaxies their light profiles were best fitted adding to the Sérsic model of Equation (1) an outer exponential function (Freeman, 1970):

$$I(r) = I_0 \exp\left(-\frac{r}{r_0}\right). \quad (2)$$

In this equation  $I_0$  is the central intensity and  $r_0$  is the length scale. The inclusion of this equation in the fitting function does not necessarily means that the galaxy has a disk component in the usual sense of rotation-supported stellar system.

We have chosen the exponential function since it is the simplest function to account for the "extra-light" observed in the above mentioned galaxies. It is worth to mention that we also tried

with a second Sérsic function since it has three degrees of freedom instead two. However, in terms of the  $\chi^2$  coefficient it is not better than the Sérsic plus exponential fit. Figure 1 shows a good example: the case of BCG A0690 where clearly a single Sérsic function cannot account for the concavity of the luminosity profile. Even when the fitting becomes adequate at the faint end of the profile, the model cannot reproduce the surface magnitude in the interval between 7 and 15 kpc, which corresponds to a surface magnitude in the range of  $21\text{--}22 \text{ mag arcsec}^{-2}$ . Error bars in this region have approximately the size of the squares. On the other hand, Figure 2 shows a much better fit due to the inclusion of the exponential component (dashed line) in the fitting model. We show that the  $21\text{--}22 \text{ mag arcsec}^{-2}$  region is now in perfect agreement with the model and the fitting functions can also properly describe the faint end of the luminosity profile. In fact, the reduced  $\chi^2$  coefficient we obtain with a Sérsic + Exponential model is about one order of magnitude smaller than those obtained with the single Sérsic fit. As a general rule, for most of those cases that are initially fitted with the single Sérsic function and in which  $n > 8$  and  $r_e > 300 \text{ kpc}$ , it is necessary to include the exponential component to obtain a proper fit.

Intensity parameters are then converted into surface brightness, expressed in  $\text{mag arcsec}^{-2}$  by the equation  $m = -2.5 \log(I)$ , while units of  $r_e$ , and  $r_0$  are converted to kpc. Errors for  $r_e$  and  $r_0$  are smaller than 15% while for  $\mu_e$ , and  $\mu_0$  errors are below  $0.20 \text{ mag arcsec}^{-2}$ . Total luminosities of both Sérsic and the exponential components are finally computed using the derived photometric parameters and integrating separately both components of Equations (1) and (2) as follows:

$$L = \int_0^\infty I(r) 2\pi r dr, \quad (3)$$

which yields

$$L_{Sersic} = I_e r_e^2 \pi \frac{2 \exp(b)}{\beta k^{2/\beta}} \Gamma(2/\beta) \quad (4)$$

for the Sérsic component and

$$L_{exp} = 2\pi I_0 r_0^2 \quad (5)$$

for the exponential component.  $\Gamma(2/\beta)$  is the gamma function. Total apparent magnitudes

are then converted into absolute magnitudes. Throughout this paper we assume a Hubble constant  $H_0 = 70 \text{ km s}^{-1} \text{ Mpc}^{-1}$  together with  $\Omega_M = 0.27$  and  $\Omega_\Lambda = 0.73$ .

## 5. Results and Discussion

Table 2 lists the photometric parameters obtained through the fitting procedure described in Section 3 for all BCGs of the sample. Columns 1-6 list the Abell BCG name, Sérsic parameters  $\mu_e$ ,  $r_e$ ,  $n$ , exponential parameters  $\mu_0$  and  $r_0$ . Columns 7-10 give absolute magnitude of the Sérsic component, absolute magnitude of the exponential component, total absolute magnitude of the BCG and Sérsic to exponential component light ratio. Column 11 contains the logarithmic slope of the metric luminosity or  $\alpha$  parameter which is defined as  $\alpha = d(\text{Log}(L_m))/d(\log(r_m))$ , where  $L_m$  is the total BCG luminosity within a circular aperture of radius  $r_m$  centered on the BCG nucleus. Following Postman & Lauer (1995) we have calculated this parameter at  $r = 14.5 \text{ kpc}$ . Columns 12-15 list the inner ellipticity (measured at  $10''$ ), outer ellipticity (measured at  $\sim 23 - 24 \text{ mag arcsec}^{-2}$ ), and inner and outer position angles of the isophotes where the ellipticities are measured. Position angles are from north to east and the typical observed errors are  $\sim 5^\circ$ , while typical errors for ellipticities are 0.06. Finally, column 16 lists the metric absolute magnitude also calculated at  $r = 14.5 \text{ kpc}$ .

The data above show that 225 out of 430 BCGs, or 52% of the sample, have a single Sérsic luminosity profile, while the remaining 205 BCGs (48%) need a double component of Sérsic + exponential to properly fit their luminosity profiles. We note that we find 27 galaxies ( $\sim 6\%$  of the whole sample) that have  $n < 1.5$  for the inner Sérsic component, which is nearer to an exponential rather than a de Vaucouleurs profile ( $n \sim 4$ ). Moreover, all but three, have double component luminosity profiles. This is particularly interesting since it has been suggested that BCGs usually have high Sérsic indices (Graham et al. 1996). However, Seigar et al. (2007) observe an inner exponential behavior in 3 out of 5 galaxies of their sample, suggesting that this may be more common in cD galaxies than previously thought. A visual inspection of these galaxies reveals that they have high

ellipticities. We calculated an average outer ellipticity  $e = 0.32 \pm 0.09$ , which is slightly higher than the average found for double profile BCGs (see the next section).

In general terms we have also noticed that the inner components of the double profile BCGs have effective radii  $r_e \sim 1 - 10 \text{ kpc}$  and Sérsic indices  $n \sim 1 - 6$ , being the averages  $r_e = 5 \pm 4 \text{ kpc}$  and  $n = 3.7 \pm 1.5$  respectively. These values are quite similar to those reported by Gonzalez et al. (2003) in their preliminary paper for a sample of 31 BCGs. However, these authors use a different approach to fit the luminosity profiles. They use two Sérsic functions instead of our Sérsic + exponential approach.

### 5.1. Single Profile BCGs versus Double Profile BCGs

A question that arises after our analysis is to establish if single profile BCGs actually differ in morphology from double profile BCGs. The models of the light profiles we apply do not imply conjectures on galaxy morphologies. Are BCGs with single and double profile of a different nature? If so, is this difference environmental or intrinsic?

In order to answer these questions we carried out a series of tests in which we explored BCGs properties together with the global cluster properties. One of them is the Kormendy relation (KR; Kormendy 1977) which is presented in Figure 3. This is an empirical scaling relation between surface brightness  $\mu_e$  and effective radius  $r_e$  and it represents the projection of the Fundamental Plane (Djorgovski & Davies 1987). For the case of single profile BCGs both  $\mu_e$  and  $r_e$  are directly obtained from the fitting profile. However, in the case of double profile BCGs, we calculate these parameters from the double profile, i.e., using the sum of the Sérsic and exponential profiles. A linear regression applied to the whole sample gives

$$\mu_e = 18.72(\pm 0.06) + 3.13(\pm 0.05) \log(r_e/\text{kpc})$$

The slope of the KR obtained for all BCGs is  $a_{BCG} = 3.13 \pm 0.05$  which is similar to the value obtained by Oegerle & Hoesel (1991) for a sample of 43 BCGs (i.e.,  $a_{BCG} = 3.12 \pm 0.14$ ).

However, Bildfell et al. (2008) obtain for a sample of BCGs selected from 48 X-ray luminous clus-

ters ( $a_{BCG} = 3.44 \pm 0.13$ ), which is considerably steeper than our value and than the value of "normal" ellipticals  $a_{ellip} = 3.02 \pm 0.14$  (Oegerle & Hoesel, 1991). Nevertheless, when we apply the same analysis to single profile and double profile BCGs separately we obtain for single profile BCGs

$$\mu_e = 18.65(\pm 0.07) + 3.29(\pm 0.06) \log(r_e/\text{kpc})$$

and for double profile BCGs

$$\mu_e = 19.03(\pm 0.10) + 2.79(\pm 0.08) \log(r_e/\text{kpc}).$$

Different slopes suggest that the formation timescale of the single profile BCGs could differ from their double profile counterpart (von der Linden et al. 2007).

It is interesting to note that these values are calculated integrating the galaxy luminosity profiles up to infinity. If we consider a finite radius instead, total luminosities will change and therefore both  $r_e$  and  $\mu_e$  will also change. We then have also calculated the KR for both subsamples considering different galaxy radii ( $r = 100, 200, 300$  kpc). We observed that the slope of the KR flattens for smaller radii and tends to a similar value for both subsamples ( $a \sim 2.6$  at  $r = 100$  kpc). This effect could easily explain the differences found in the size-luminosity relation between von der Linden et al. (2007) and Lauer et al. (2007) and Bernardi et al. (2007). von der Linden (2007) defines the  $r_e$  by integrating luminosity profiles up to the  $\mu = 23 \text{ mag arcsec}^{-2}$  isophote, while Lauer et al. (2007) and Bernardi et al. (2007) integrate the luminosity profiles up to infinity.

We also find that single profile BCGs show a median total absolute magnitude  $M_{T,single} = -23.8 \pm 0.7$ , while double profile BCGs have  $M_{T,double} = -24.0 \pm 0.5$ . The Kolmogorov-Smirnov (K-S) test applied to these data indicates that the  $M_T$  distributions for single profile and double profile BCGs are statistically different at 99.4% confidence level. Figure 4 shows the total absolute magnitude distributions for single and double profile BCGs.

To verify our findings and to rule out a possible dependence on our fitting models, we calculated the total luminosity within different diaphragms with radius ranging from 5 to 70 kpc. We find that integrated luminosities for both subsamples are indistinguishable up to  $r = 15$  kpc. This can

be seen in Figure 5 where we plot the absolute integrated magnitude versus the radius of the circular diaphragm expressed in kpc. The vertical line indicates  $r = 14.5$  kpc where metric luminosity and alpha parameter are calculated. Average integrated luminosities beyond 20 kpc are  $\sim 0.2$  mag brighter for double profile BCGs. We have applied the K-S test to both subsamples and results indicate that they do not statistically differ for  $r = 5, 10$ , and  $14.5$  kpc, while for larger radii the integrated luminosity distribution are truly different at the 99 % confidence level. We highlight that  $r = 20$  kpc is close to value for which the Sérsic component equals the exponential component (see the case for A0690 in Figure 2). From the data tabulated in Table 2, it is straightforward to compute the radius where  $I_{Sersic} = I_{exp}$  for each of the double profile BCGs. Averaging these values we find  $\langle r \rangle = 13 \pm 5$  kpc at  $\langle \mu \rangle = 22.5 \pm 0.7 \text{ mag arcsec}^{-2}$ . In other words, this result corroborates that the extra-light observed in double profile BCGs originates in the intermediate regions of the galaxies and not in the inner regions. The same conclusion can also be derived from Figure 6 where we plotted the total sum of the luminosity profiles corresponding to the single and double profile BCGs. Prior to the sum, individual profiles are normalized to their effective radii. Note that the extra-light of the double profile BCGs becomes apparent in the region  $1 < r/r_e < 5$ , which roughly correspond to  $\sim 15 - 75$  kpc.

## 5.2. Ellipticities and Isophote Twisting

We have also explored other photometric parameters which are not directly related to the surface brightness profile fitting functions. Figure 7 shows the ellipticity distributions for single and double profile BCGs, and Figure 8 shows the absolute value of the inner minus outer ellipticity distributions for the same subsamples. Outer ellipticities are measured at  $\mu \sim 23-24 \text{ mag arcsec}^{-2}$  which is approximately half a magnitude brighter than our limit surface magnitudes. Similarly, the inner ellipticity is measured at  $r \sim 4-5''$ , which corresponds to 3-4 times the average seeing. In Figure 7 we show that double profile BCGs have higher ellipticities than single profile BCGs. We obtain an average ellipticity  $\langle e_{double} \rangle = 0.30 \pm 0.10$  for double profile BCGs and  $\langle e_{single} \rangle = 0.26 \pm 0.11$  for single profile BCGs. A

K-S test applied to these data indicates that the ellipticity distributions for single and double profile BCGs are statistically different at a 98.3% confidence level. Similar results are obtained for the inner minus outer ellipticity of these subsamples. We obtain an average  $\langle \Delta e_{double} \rangle = 0.15 \pm 0.10$  for the double profile BCGs, while for single profile BCGs we have  $\langle \Delta e_{single} \rangle = 0.10 \pm 0.09$ . Again, the K-S test indicates different distributions at 99.9% confidence level. The logarithmic slope of the metric luminosity (calculated at  $r = 14.5$  kpc)  $\alpha$  is also higher in double profile BCGs ( $\langle \alpha_{double} \rangle = 0.65 \pm 0.12$ ) than in single profile BCGs ( $\langle \alpha_{single} \rangle = 0.59 \pm 0.14$ ). Figure 9 presents the distributions of  $\alpha$  for single and double profile BCGs respectively. A K-S test applied to these data establishes that the distributions are statistically different at a 99.9% confidence level.

The presence of isophote twisting was also explored. We calculated the outer minus inner position angle of the isophotes for those galaxies with ellipticities greater than 0.15 since position angle errors associated with rounder isophotes are large. We found similar values for both single and double profile BCGs ( $\langle \Delta pa \rangle = 8^\circ \pm 9^\circ$ ).

### 5.3. Sérsic + Exponential or Exponential + Sérsic?

By combining a large set of hydrodynamical simulations spanning a broad range of luminosity profiles of various masses, Hopkins et al. (2009) show an alternative way to separate luminosity profiles into an inner starburst component and outer pre-starburst component for "cusp" ellipticals which are formed via gas-rich mergers. These authors show that dissipational mergers give rise to two-component luminosity profiles which can be accounted by an exponential function (inner component) plus a Sérsic model (outer component). The exponential function accounts for the extra-light that was formed in a compact central starburst and makes the inner light profile of the galaxy deviate from a single Sérsic in the galaxy core. The outer component was formed by violent relaxation of the stars already present in the precursor galaxies.

We fitted to our double component BCGs an exponential (inner) + Sérsic (outer) model in the order proposed by Hopkins et al. (2009). As an example, we show the results of this fitting for the

BCG A0690 in Figure 10. The agreement between model and measurements is excellent and the Hopkins model properly accounts for the luminosity profile. We also compared the rms and  $\chi^2$  values with those obtained with our original Sérsic + exponential model and we find that both models are equally good. In other words, our approach and the Hopkins model are, from a mathematical point of view, equivalent.

The results of fitting exponential + Sérsic models to our double profile galaxies are summarized in Table 3, which lists the same 10 parameters as in Table 2. In this case Sérsic parameters  $\mu_e$ ,  $r_e$  and  $n$  correspond to the outer component, while the exponential  $\mu_0$  and  $r_0$  parameters correspond to the inner component. Obtained  $\chi^2$  values indicate that this fit proved to be equally good as the inner Sérsic + outer exponential form. However, for some galaxies we inexorably obtained unrealistic ( $\geq 300$  kpc) effective radius using the Hopkins model, this is not the case for the Sérsic + exponential approach. Given that our results suggest that the extra-light comes from the intermediate regions (see also the next section), we believe that the Sérsic + exponential profile fitting is the appropriate selection for the BCGs analyzed in the present work.

### 5.4. Extra-light and D-cD Envelopes

Around  $\sim 20\%$  of giant elliptical galaxies have extensive, low-luminosity envelopes. These galaxies are known as D type, and those with the largest envelopes are denominated cD galaxies (Mackie, 1992). The envelopes, which are seen as deviations from the de Vaucouleurs profile, are quite faint, occur below  $24 \text{ mag arcsec}^{-2}$  in the  $V$  band, and they extend well beyond 100 kpc in projected size. Thus, only few giant ellipticals have confirmed envelopes.

We explore if the extra-light found at intermediate radii is related to an eventual cD envelope. From the works of Kemp et al. (2007), Seigar et al. (2007), Mackie (1992), and Schombert (1986, 1987, 1988), we have found 24 BCGs, cataloged as cD galaxies with confirmed envelopes, in common with our sample. These are: A85, A150, A151, A193, A262, A358, A539, A779, A1177, A1238, A1767, A1795, A1809, A1904, A1913, A2028, A2147, A2162, A2199, A2366, A2572, A2589, A2634, and A2670. Table 2 shows that 19 (79%) of

these 24 galaxies are double profile BCGs, while 5 (21%) are single profile BCGs. Note that three galaxies (A151, A1767, and A2589) from those five single profile BCGs, have  $r_e > 100$  kpc, and  $n > 6$ . These parameters are very close (see Section 4) to the limit ( $r_e > 300$  kpc,  $n > 8$ ) where it is necessary to include an additional exponential profile to obtain a reasonable fit. On the other hand, one must also note that a visual classification as cD, does not necessarily imply the presence of an envelope. Schombert (1986), and Seigar et al. (2007) cataloged A496, A505, A1691, A2029, A2052, A2107, A2197, and A2666, as cDs without envelopes. For all those galaxies, except A2197, our surface profile modeling is consistent with just one component.

These results strongly suggest that the extra-light found in double component BCGs at intermediate radii is related to the faint envelope. Moreover, they indicate that this component is not only confined to the outskirts of the parent galaxy. Galaxy halos generally considered an outer component in galaxy structure appear to originate in the inner regions of BCGs.

### 5.5. BCGs Morphologies and IR Emission

Although a visual inspection of our BCGs suggests that they all are early-type galaxies, we probe the possibility that the differences we observe in the profiles are due to actual differences in the morphology. The Galaxy Zoo project (<http://zoo1.galaxyzoo.org/>) provides the morphological types for a large sample of galaxies observed by the Sloan Digital Sky Survey (SDSS; Lintott et al. 2010). In this catalog 66 of the BCGs studied here have a morphological classification: 31 (47%) are single profile BCGs, while 35 (53%) are double profile BCGs. The Lintott et al. (2010) catalog gives the probability that a particular galaxy is an early-type galaxy or late-type (spiral) galaxy. We find that both single and double profile BCGs have the same probability to be classified as elliptical galaxies in the Galaxy Zoo catalog. However, from the 31 single profile BCGs with morphological classification only 5 (16%) belong to the 'unknown' category, while for the 35 double profile BCGs in the catalog this number rises up to 9 (26%). It is also interesting to note that a visual inspection of these nine double profile BCGs with unknown morphology are

mostly interacting galaxies with two or three near companions, while the five single profile BCGs with unknown classification appear to us as normal ellipticals.

We have scrutinized the infrared emission of a subsample of our BCGs using data from Quillen et al. (2008). They report on an imaging survey with the *SpitzerSpaceTelescope* of 62 BCGs with optical line emission. We have 12 BCGs in common with Quillen et al. (2008), 6 having single component luminosity profiles and 6 having double component luminosity profiles. Analysis of the 24-8  $\mu$ m flux ratios shows that only one (17%) of single profile BCG (A2052) have infrared excess, while for double profile BCGs this number increases to 4 (67%). Infrared excess is a star formation signature. In fact, O'Dea et al. (2010) in their study of seven BCGs using *HubbleSpaceTelescope*(*HST*) ultra-violet and *Spitzer* infrared data found that all these galaxies have extended UV continuum and  $L - \alpha$  emission as well as an infrared excess. Based on their findings O'Dea et al. (2010) confirm that the BCGs they study are actively forming stars. Moreover, they suggest that the IR excess is indeed associated with star formation and they also confirm that the FUV continuum emission extends over a region  $\sim 7$ -28 kpc. Although these results are only for a few BCGs in our sample, they suggest that the "extra-light" observed in the double profile BCGs indicates active star formation in the intermediate regions of these galaxies.

### 5.6. Global Cluster Properties

In this section we compare BCGs properties to those of the host cluster such as cluster X-ray luminosity, the projected distance of the BCG with respect to the center of the X-ray emission and the BCG position angle with respect to that of the cluster. We have used data taken from Ledlow et al. (2003) to determine the offset in kpc between the X-ray peak and the optical position of the BCG. X-ray cluster luminosities were taken from Sadat et al. (2004) data, while the position angle of the clusters are obtained from Plionis (1994), Rhee & Katgert (1987), and Binggeli (1982). In this case we have only selected those clusters with ellipticities  $> 0.15$ , since for smaller ellipticities position angles have large errors.



Single and double profile BCGs have similar orientations relative to the whole cluster and X-ray luminosity distributions. We did not observe any difference between the single profile and double profile BCG samples with respect to the cluster position angle and X-ray cluster luminosity. However, Bildfell et al. (2008) report that brighter BCGs are located closer to the X-ray peak emission. In our case, considering that on average double profile BCGs are brighter than single profile BCGs we should observe larger offsets in single profile BCGs. Nevertheless, we find no significant differences between single profile and double profile BCGs offsets with respect to the X-ray center emission of the cluster. Moreover, we do not find any correlation between the total absolute magnitude and X-ray offset. Figure 11 shows that there is no obvious trend between the total absolute magnitude of both single profile and double profile BCGs.

## 6. Conclusions

We have established the existence of two sub-populations of BCGs based on their luminosity profiles. We analyze a uniquely large sample of 430 BCGs and find that 48% of these galaxies have a light profile that deviates from the standard single Sérsic model. The luminosity profiles of these galaxies are in fact better described by a double component model consisting of an inner Sérsic profile and an outer exponential component. The necessity of an outer exponential component conveys the presence of extra-light at intermediate radii corresponding to surface magnitudes  $\sim 22 \text{ mag arcsec}^{-2}$ . We have found strong evidence from a subsample of 24 BCGs that extra-light is closely related to the presence of a faint envelope. Similarly, from other subsample of 12 BCGs we also found evidence that links extra-light and star formation.

This work highlights the need to cover a large spatial scale when deriving the structural parameters of large galaxies. Accurate parameters can only be obtained when the entire galaxy is considered and this often requires the creation of composite light profiles using data from different telescopes as clearly illustrated by Kormendy et al. (2009). *HST* detectors provide a superb spatial resolution that has been fundamental for the study

of the deviation from the Sérsic law of the light profile in the inner regions of galaxies i.e. cusps and evacuated cores (Ferrarese et al. 2006). However, *HST* detectors do not provide the field of view necessary to truthfully derive the structural parameters of galaxies with a light profile that deviates from a single Sérsic law at large radii.

## 7. Acknowledgments

We are thankful to M. Postman (STScI) for giving us access to the data used in this study. We also wish to thank the anonymous referee for his useful comments which helped to clarify and strengthen this paper. This research has made use of the NASA Astrophysics Data System Bibliographic services (ADS) and the NASA/IPAC Extragalactic Database (NED) which is operated by the Jet Propulsion Laboratory, California Institute of Technology, under contract with the National Aeronautics and Space Administration. This work has been partially supported with grants from Consejo Nacional de Investigaciones Científicas y Técnicas de la República Argentina (CONICET), Secretaría de Ciencia y Tecnología de la Universidad de Córdoba and Ministerio de Ciencia y Tecnología de Córdoba, Argentina.

Bernardi, M., Hyde, J.B., Sheth, R.K., Miller, C.J., Nichol, R.C. 2007, *AJ*, 133, 1741

Bildfell, C.; Hoekstra, H.; Babul, A.; Mahdavi, A. 2008, *MNRAS*, 389, 1637

Binggeli, B. 1982, *A&A*, 107, 338

Caon, N., Capaccioli, M., & D’Onofrio, M. 1993, *MNRAS*, 265, 1013

Coenda, V., Donzelli, C.J., Muriel, H., Quintana, H., & Infante, L. 2005, *AJ*, 129, 1237

Conroy, C., Wechsler, R. H., & Kravtsov, A. V. 2007, *ApJ*, 668, 826

de Lucia, G. & Blaizot, J. 2007, *MNRAS*, 375, 2

de Vaucouleurs, G. 1948, *Ann. Astrophys.*, 11, 247

- Djorgovski, S., & Davis, M. 1987, *ApJ*, 313, 59
- Donzelli, C.J., Chiaberge, M., Macchetto, F. D., Madrid, J.P., Capetti, A., & Marchesini, D. 2007, *ApJ*, 667, 780
- Ferrarese, L., et al. 2006, *ApJS*, 164, 334
- Freeman, K. C. 1970, *ApJ*, 160, 811
- Gonzalez, A. H., Zabludoff, A. I., & Zaritsky, D. 2003, *Ap&SS*, 285, 67
- Gonzalez, A. H., Zabludoff, A. I., & Zaritsky, D. 2005, *ApJ*, 618, 195
- Graham, A.W., & Driver, S.P. 2005, *PASA*, 22, 118
- Graham, A.W., Lauer, T.R., Colless, M. & Postman, M. 1996, *ApJ*, 465, 534
- Hopkins, P.F., Cox, T. J., Dutta, S. N., Hernquist, Lars., Kormendy, J., Lauer, T. R. 2009, *ApJS*, 181, 135
- Jedrzejewski, R. 1987, *MNRAS*, 226, 747
- Kent, S.M. 1985, *ApJS*, 59, 115
- Kent, S.N., Guzmán Jiménez, V., Ramírez Beraud, P., Hernández Ibarra, F.J., & Pérez Grana, J.A. 2007, in *IAU Symp. 235, Galaxy Evolution Across the Hubble Time*, ed. F. Combes & J. Palous (Cambridge: Cambridge Univ. Press), 213
- Kormendy, J. 1977, *ApJ*, 218, 333
- Kormendy, J., Fisher, D. B., Cornell, M. E., & Bender, R. 2009, *ApJS*, 182, 216
- La Barbera, F., Busarello, G., Merluzzi, P., De La Rosa, I., Coppola, G., & Haynes, C.P. 2008, *PASP*, 120, 681
- Landolt, A.U. 1983, *AJ*, 88, 853
- Lauer, T. R., & Postman, M. 1992, *ApJ*, 400, L50
- Lauer, T.R., et al. 2007, *ApJ*, 662, 808
- Ledlow, M.J., Voges, W., Owen, F.N., & Burns, J.O. 2003, *AJ*, 126, 2740
- Lintott, C. et al. 2011, *MNRAS*, 410, 166
- Lugger, P.M. 1984, *ApJ*, 286, 106
- Mackie, G. 1992, *ApJ*, 400, 65
- Oegerle, W.R.; Hoessel, J.G. 1991, *ApJ*, 375, 150
- O’Dea, K. et al. 2010, *ApJ*, 719, 1619
- Plionis, M. 1994, *ApJS*, 95, 401
- Postman, M. & Lauer, T. R. 1995, *ApJ*, 440, 28
- Quillen, A.C. et al. 2008, *ApJS*, 176, 39
- Rhee, G., & Katgert, P. 1987, *A&A*, 183, 217
- Sadat, R., Blanchard, A., Kneib, J.P., Mathez, G., Madore, B., & Mazzarella, J.M. 2004, *A&A*, 424, 1097
- Seigar, M.S., Graham, A.W., Jerjen, H. 2007, *MNRAS*, 378, 1575
- Schombert, J.M. 1986, *ApJS*, 60, 603
- Schombert, J.M. 1987, *ApJS*, 64, 643
- Schombert, J.M. 1988, *ApJ*, 328, 475
- Schombert, J.M. & Bothun, G.D. 1987, *AJ*, 93, 60
- Sérsic, J.L. 1963, *Boletín de la Asociación Argentina de Astronomía*, 6, 41
- Sérsic, J.L. 1968, *Atlas de Galaxias Australes*

(Córdoba: Obs. Astronóm.)

von der Linden, A., Best, P.N., Kauffmann, G.,  
& White, S. 2007, MNRAS, 379, 867

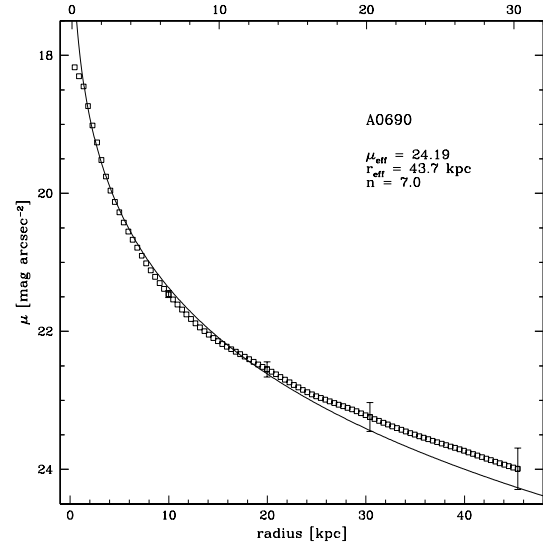


Fig. 1.— BCG A0690 luminosity profile with the single Sérsic fitting. Upper scale is in arcsec.

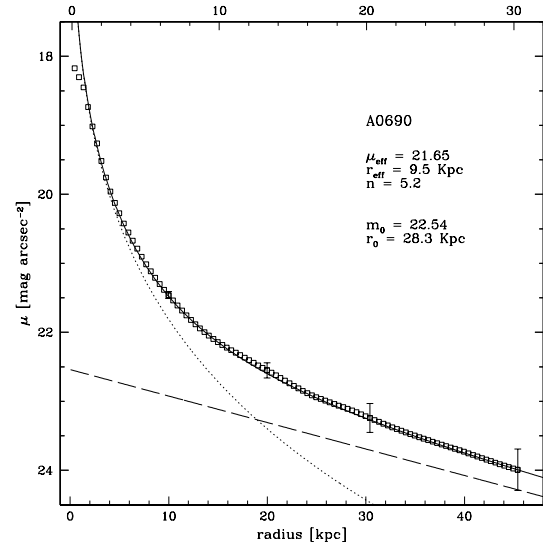


Fig. 2.— Inner Sérsic (short dashed line) + outer exponential (long dashed line) fitting model for A0690 luminosity profile.

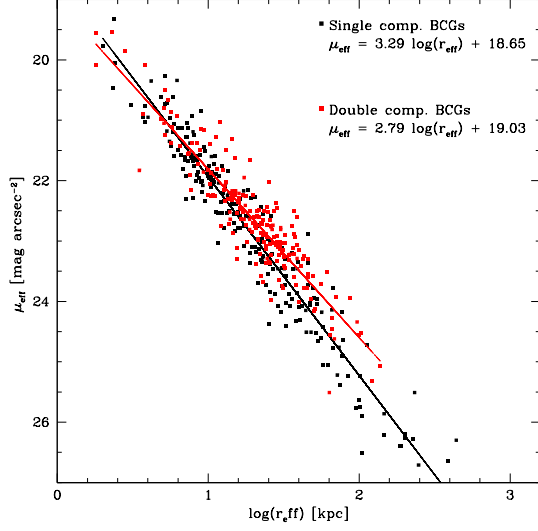


Fig. 3.— Kormendy relation for sample galaxies. Black dots represent single profile BCGs, while red dots represent double profile BCGs. Best fits for both subsamples are also shown.

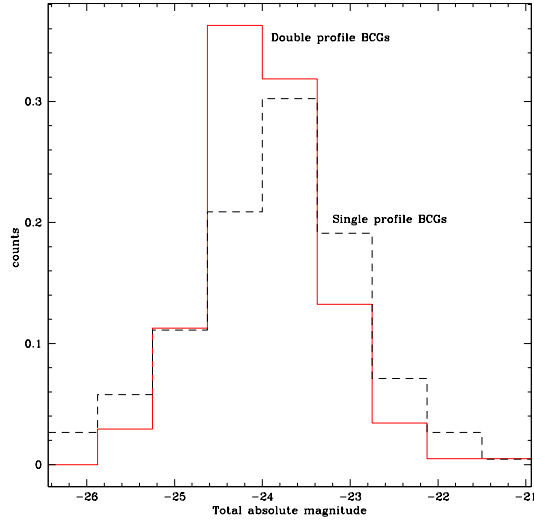


Fig. 4.— Total magnitude distributions for single (black line) and double profile (red line) BCGs.

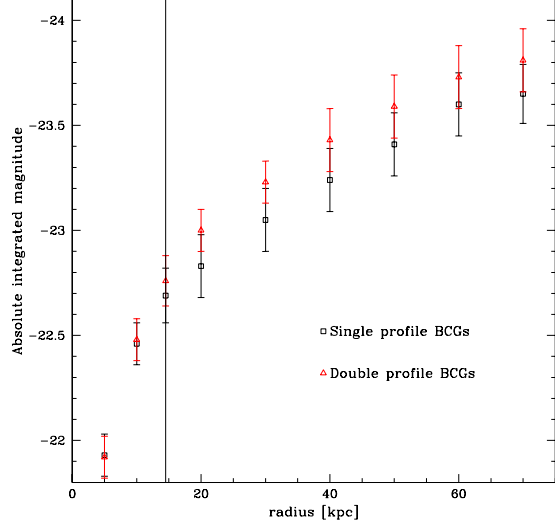


Fig. 5.— Integrated absolute magnitudes vs. diaphragm radius in kpc. The vertical line indicates where alpha parameter and metric magnitudes are calculated.

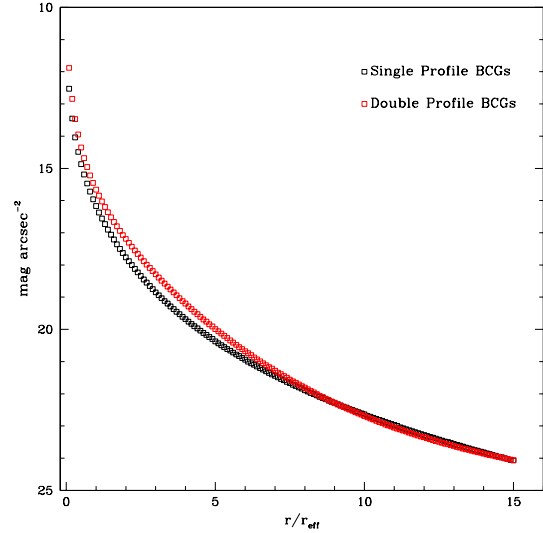


Fig. 6.— Luminosity profiles obtained using the stacking technique for all single and double profile BCGs. Prior to the stacking the individual profiles were normalized at the effective radius.

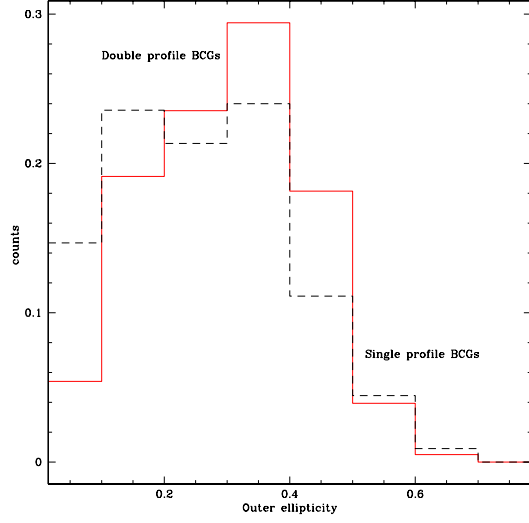


Fig. 7.— Outer ellipticity distributions for single (black line) and double profile (red line) BCGs.

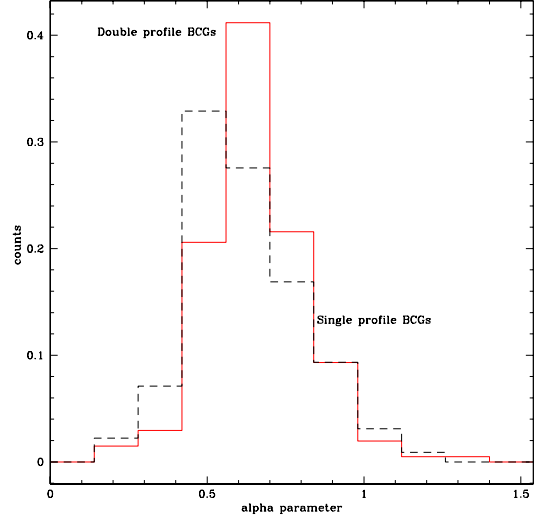


Fig. 9.—  $\alpha$  parameter distributions for single (black line) and double profile (red line) BCGs.

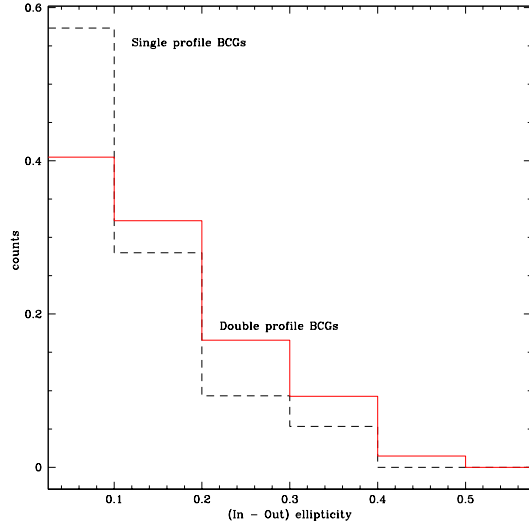


Fig. 8.— Outer minus inner ellipticity distributions for single (black line) and double profile (red line) BCGs.

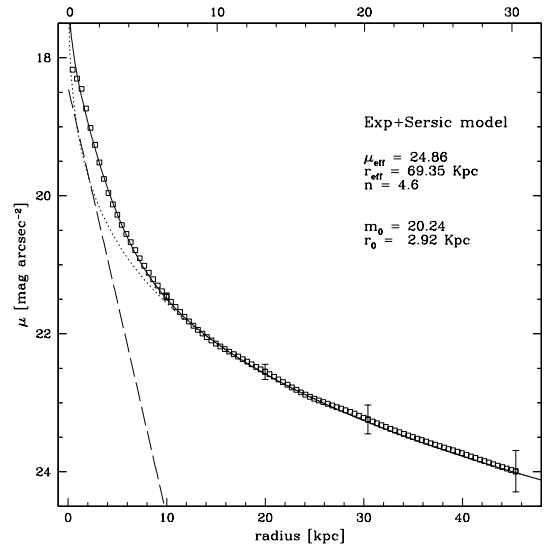


Fig. 10.— Exp + Sérsic model fit for A0690 luminosity profile. Outer Sérsic (short dashed line) and inner exponential (long dashed lined) can be observed.

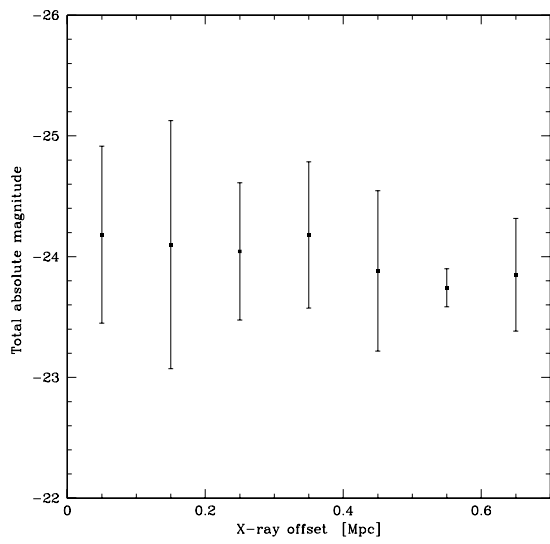


Fig. 11.— BCGs total absolute magnitude vs. X-ray offset for the whole BCG sample.

TABLE 1  
BCGs IMAGING RUNS

Run	Date	Observatory	Pixel Scale (")	FOV (')
1	1989 Oct	CTIO	0.273	3.6
2	1989 Nov	KPNO 4m	0.299	4.0
3	1990 Nov	CTIO	0.273	3.6
4	1991 Mar	KPNO 2.1m	0.304	5.2
5	1991 Apr	CTIO	0.434	7.4
6	1993 Sep	KPNO 2.1m	0.304	5.2
7	1993 Nov	CTIO	0.434	7.4
8	1994 May	KPNO 2.1m	0.304	5.2
9	1994 May	CTIO	0.434	7.4
10	1994 Oct	KPNO 2.1m	0.304	5.2
11	1994 Dec	CTIO	0.434	7.4
12	1995 Apr	CTIO	0.434	7.4
13	1995 Apr	KPNO 2.1m	0.304	5.2

TABLE 2  
BCGs PHOTOMETRICAL PARAMETERS

Name (1)	$\mu_e$ (2)	$r_e$ (3)	$n$ (4)	$\mu_0$ (5)	$r_0$ (6)	$M_{Sersic}$ (7)	$M_{exp}$ (8)	$M_T$ (9)	$S/e$ (10)	$\alpha$ (11)	$e_{in}$ (12)	$e_{out}$ (13)	$pa_{in}$ (14)	$pa_{out}$ (15)	$M_{metric}$ (16)
A0014	26.65	387.58	5.08	—	—	-26.65	0.00	-26.65	—	1.10	0.35	0.56	56.5	52.0	-22.87
A0027	24.41	32.51	7.58	—	—	-23.67	0.00	-23.67	—	0.59	0.24	0.28	-54.0	-61.2	-22.18
A0071	20.73	5.18	5.49	—	—	-23.28	0.00	-23.28	—	0.49	0.06	0.05	51.1	31.1	-22.45
A0074	23.24	23.04	6.45	—	—	-24.05	0.00	-24.05	—	0.54	0.28	0.30	42.2	39.6	-22.93
A0075	21.86	10.58	4.74	—	—	-23.55	0.00	-23.55	—	0.55	0.09	0.23	85.0	60.4	-22.74
A0076	24.08	34.80	7.58	—	—	-24.09	0.00	-24.09	—	0.57	0.05	0.17	-66.4	-118.7	-22.80
A0077	26.39	190.00	6.94	—	—	-25.65	0.00	-25.65	—	0.91	0.13	0.51	-62.5	-64.0	-23.04
A0080	21.59	5.92	2.24	—	—	-22.29	0.00	-22.29	—	0.46	0.11	0.06	-64.2	-71.0	-21.98
A0085	21.43	12.43	0.86	21.63	26.00	-23.47	-24.24	-24.68	0.49	1.30	0.11	0.35	-27.3	-32.1	-23.18
A0086	22.55	14.89	6.17	—	—	-23.76	0.00	-23.76	—	0.56	0.26	0.17	70.6	74.8	-22.90
A0102	23.73	32.22	7.41	—	—	-24.36	0.00	-24.36	—	0.61	0.13	0.11	-64.2	-41.3	-22.97
A0114	22.73	20.87	5.85	—	—	-24.26	0.00	-24.26	—	0.59	0.16	0.28	72.9	73.6	-23.01
A0116	21.44	9.44	4.52	—	—	-23.74	0.00	-23.74	—	0.58	0.17	0.17	5.5	15.5	-22.93
A0117	24.06	47.47	6.06	—	—	-24.73	0.00	-24.73	—	0.76	0.12	0.28	-7.7	-19.9	-23.20
A0119	26.71	247.61	7.87	—	—	-25.77	0.00	-25.77	—	0.83	0.12	0.33	34.8	35.9	-23.01
A0126	20.74	3.10	3.61	—	—	-21.78	0.00	-21.78	—	0.26	0.04	0.09	-38.6	38.9	-21.55
A0133	21.10	7.64	1.11	21.46	23.80	-22.87	-24.23	-24.50	0.29	0.93	0.07	0.43	33.7	22.4	-22.95
A0134	21.19	5.86	4.72	—	—	-22.98	0.00	-22.98	—	0.47	0.14	0.05	10.5	1.6	-22.40
A0147	21.75	10.17	6.06	—	—	-23.64	0.00	-23.64	—	0.49	0.16	0.09	33.6	31.6	-22.83
A0150	20.93	6.34	1.91	22.01	26.20	-22.91	-23.89	-24.26	0.40	0.75	0.11	0.43	-2.9	-4.8	-22.81
A0151	25.86	146.25	8.06	—	—	-25.51	0.00	-25.51	—	0.78	0.17	0.26	73.5	76.9	-23.11
A0152	18.92	1.38	5.65	20.93	11.80	-22.24	-23.32	-23.66	0.37	0.84	0.04	0.28	39.0	17.2	-22.64
A0154	21.82	11.13	5.21	22.33	28.00	-23.76	-23.72	-24.50	1.04	0.66	0.22	0.39	-38.9	-44.1	-23.05
A0158	19.06	1.66	4.15	20.97	10.20	-22.28	-22.90	-23.39	0.56	0.71	0.13	0.12	-59.4	-48.6	-22.58
A0160	20.38	3.04	1.04	21.05	12.50	-21.49	-23.18	-23.38	0.21	0.78	0.03	0.24	-73.1	-92.1	-22.44
A0161	20.53	3.65	4.74	22.33	23.50	-22.64	-23.40	-23.84	0.50	0.67	0.05	0.31	4.9	-42.9	-22.07
A0168	24.51	48.01	7.41	—	—	-24.38	0.00	-24.38	—	0.65	0.06	0.25	-25.6	-26.5	-22.83
A0171	22.75	17.23	6.49	—	—	-24.04	0.00	-24.04	—	0.63	0.14	0.12	86.5	30.7	-23.00
A0174	20.44	3.71	0.98	21.56	13.02	-21.97	-22.89	-23.27	0.43	0.66	0.02	0.16	5.9	-64.9	-22.53
A0179	21.14	5.27	3.73	21.92	16.30	-22.62	-22.93	-23.54	0.75	0.63	0.22	0.38	-27.3	-25.6	-22.35
A0189	21.13	7.32	3.06	—	—	-23.15	0.00	-23.15	—	0.40	0.42	0.50	-2.8	-6.7	-22.24
A0193	18.60	1.78	4.13	21.52	22.00	-22.84	-23.97	-24.30	0.36	0.59	0.04	0.23	-69.9	-73.3	-22.88
A0194	18.59	1.30	1.53	19.95	7.70	-21.51	-23.12	-23.34	0.23	0.68	0.25	0.36	56.6	60.5	-22.58
A0195	21.62	8.16	6.58	—	—	-23.42	0.00	-23.42	—	0.50	0.09	0.05	-84.7	11.2	-22.69
A0208	21.66	7.95	5.32	22.36	26.80	-23.37	-23.76	-24.34	0.70	0.67	0.06	0.33	10.7	25.5	-22.95
A0225	25.24	84.64	7.09	—	—	-24.95	0.00	-24.95	—	0.78	0.15	0.27	81.2	81.6	-22.92
A0240	24.61	55.91	5.38	—	—	-24.50	0.00	-24.50	—	0.86	0.09	0.21	4.6	9.3	-22.74
A0245	21.95	8.70	3.28	—	—	-23.02	0.00	-23.02	—	0.57	0.21	0.27	-65.2	-81.4	-22.30
A0246	23.73	24.12	6.33	—	—	-23.70	0.00	-23.70	—	0.62	0.16	0.39	17.8	11.0	-22.42
A0257	19.86	2.99	4.26	21.13	11.90	-22.91	-23.21	-23.83	0.75	0.64	0.26	0.42	9.9	24.1	-22.76
A0260	20.95	6.17	4.50	21.85	20.90	-23.17	-23.46	-24.08	0.76	0.62	0.12	0.33	46.3	73.2	-22.89
A0261	20.19	4.08	2.60	21.69	15.30	-22.79	-23.00	-23.65	0.83	0.57	0.10	0.18	-2.7	-9.8	-22.81
A0262	20.33	3.18	1.75	21.16	16.60	-21.54	-23.33	-23.52	0.19	0.76	0.07	0.41	-73.6	42.0	-22.21
A0267	25.90	105.21	6.29	—	—	-24.66	0.00	-24.66	—	0.90	0.19	0.33	78.4	72.0	-22.58
A0268	20.23	2.85	3.70	22.80	14.30	-22.31	-21.89	-22.88	1.47	0.47	0.14	0.27	2.7	-11.5	-22.06
A0279	22.81	18.86	5.29	22.56	30.60	-24.01	-23.76	-24.65	1.25	0.81	0.11	0.24	40.2	47.6	-23.10
A0292	23.37	45.49	3.11	—	—	-25.01	0.00	-25.01	—	0.88	0.31	0.58	-84.9	-85.6	-22.94
A0295	21.47	4.64	2.99	21.44	17.30	-21.84	-23.48	-23.70	0.22	0.66	0.11	0.44	76.4	67.0	-22.76
A0311	22.79	15.71	5.43	22.36	38.00	-23.59	-24.38	-24.81	0.48	0.80	0.17	0.53	15.7	29.0	-22.83
A0326	21.06	5.91	3.14	—	—	-22.87	0.00	-22.87	—	0.38	0.42	0.11	21.5	87.7	-22.22
A0347	20.95	3.99	3.66	—	—	-21.82	0.00	-21.82	—	0.32	0.30	0.21	-76.7	-66.5	-21.28
A0357	21.61	7.00	2.51	—	—	-22.68	0.00	-22.68	—	0.35	0.41	0.47	-42.1	-39.9	-21.85
A0358	23.57	32.81	5.13	—	—	-24.34	0.00	-24.34	—	0.76	0.17	0.28	3.9	11.0	-22.87
A0376	25.76	94.82	8.00	—	—	-24.66	0.00	-24.66	—	0.73	0.05	0.27	-82.9	81.7	-22.71
A0396	20.47	2.35	1.66	—	—	-20.87	0.00	-20.87	—	0.22	0.47	0.35	7.7	7.7	-20.42
A0397	20.31	3.82	3.44	21.78	19.20	-22.66	-23.38	-23.83	0.51	0.61	0.14	0.40	39.2	60.5	-22.87
A0399	21.82	10.41	1.22	21.83	33.30	-22.92	-24.65	-24.85	0.20	1.13	0.23	0.43	46.5	39.8	-22.80
A0401	28.27	968.92	7.46	—	—	-27.25	0.00	-27.25	—	1.02	0.26	0.58	35.8	24.7	-23.01



TABLE 2—*Continued*

Name (1)	$\mu_e$ (2)	$r_e$ (3)	$n$ (4)	$\mu_0$ (5)	$r_0$ (6)	$M_{Sersic}$ (7)	$M_{exp}$ (8)	$M_T$ (9)	$S/e$ (10)	$\alpha$ (11)	$e_{in}$ (12)	$e_{out}$ (13)	$pa_{in}$ (14)	$pa_{out}$ (15)	$M_{metric}$ (16)
A0404	20.33	4.04	1.09	21.26	12.40	-22.27	-23.03	-23.47	0.50	0.62	0.27	0.37	22.4	24.7	-22.57
A0415	22.20	9.26	3.88	21.95	26.00	-22.91	-24.02	-24.36	0.36	0.86	0.12	0.32	-20.1	-12.5	-22.72
A0419	21.68	7.33	4.55	—	—	-22.85	0.00	-22.85	—	0.40	0.28	0.32	-61.2	-25.0	-22.06
A0423	25.05	61.90	6.80	—	—	-24.48	0.00	-24.48	—	0.70	0.19	0.47	-75.5	-70.3	-22.56
A0428	18.82	1.65	3.51	21.71	6.80	-22.43	-21.29	-22.75	2.86	0.41	0.03	0.09	8.0	48.6	-22.18
A0450	22.01	8.26	4.35	—	—	-22.92	0.00	-22.92	—	0.49	0.21	0.16	12.5	-2.2	-22.25
A0496	25.74	101.00	5.62	—	—	-24.57	0.00	-24.57	—	0.78	0.16	0.37	-8.6	-3.9	-22.75
A0497	20.95	2.41	3.58	21.51	9.70	-21.31	-22.44	-22.77	0.35	0.81	0.20	0.28	26.5	31.0	-21.95
A0500	20.90	5.92	2.90	22.44	30.00	-23.03	-23.79	-24.23	0.50	0.63	0.21	0.37	9.0	33.0	-22.83
A0505	24.64	78.09	6.80	—	—	-25.29	0.00	-25.29	—	0.84	0.14	0.17	-51.9	11.0	-23.39
A0514	23.13	21.69	5.56	—	—	-23.98	0.00	-23.98	—	0.61	0.19	0.31	-53.3	-49.9	-22.90
A0533	22.59	16.32	4.98	—	—	-23.75	0.00	-23.75	—	0.55	0.24	0.17	-61.2	-44.8	-22.69
A0536	25.23	84.14	6.54	—	—	-25.15	0.00	-25.15	—	0.84	0.29	0.41	-34.1	-29.2	-23.05
A0539	21.03	5.56	4.76	22.31	22.30	-22.91	-23.15	-23.79	0.80	0.50	0.04	0.36	-11.3	-2.0	-22.59
A0543	19.33	2.39	2.48	—	—	-22.63	0.00	-22.63	—	0.27	0.07	0.02	-64.1	-47.6	-22.06
A0548	21.41	7.07	4.08	20.39	6.60	-22.98	-22.45	-23.50	1.63	0.64	0.34	0.14	64.4	82.7	-22.73
A0550	22.20	10.71	4.26	23.00	51.50	-23.33	-24.52	-24.83	0.34	0.76	0.15	0.38	-43.4	-56.8	-22.79
A0553	21.69	9.57	3.44	23.30	57.80	-23.48	-24.46	-24.83	0.40	0.57	0.16	0.57	-68.4	-67.1	-22.87
A0564	20.09	3.86	1.28	23.03	29.20	-22.64	-23.28	-23.76	0.55	0.39	0.23	0.35	29.5	42.1	-22.54
A0568	21.59	11.11	2.87	—	—	-23.84	0.00	-23.84	—	0.69	0.18	0.11	31.9	-22.7	-23.07
A0569	22.11	13.01	4.72	—	—	-23.22	0.00	-23.22	—	0.50	0.13	0.15	-4.4	34.3	-22.54
A0576	20.35	4.19	4.74	—	—	-22.94	0.00	-22.94	—	0.32	0.17	0.08	-60.2	46.9	-22.37
A0582	20.38	3.79	4.88	22.95	26.60	-22.92	-23.09	-23.76	0.86	0.51	0.01	0.04	-52.3	16.2	-22.63
A0592	20.55	4.44	4.29	22.00	13.30	-22.17	-21.67	-22.70	1.58	0.52	0.07	0.21	84.6	-86.6	-22.58
A0595	21.76	7.99	5.62	—	—	-23.27	0.00	-23.27	—	0.49	0.06	0.16	76.2	78.8	-22.51
A0600	23.54	24.95	4.52	—	—	-23.89	0.00	-23.89	—	0.73	0.10	0.35	26.8	-1.1	-22.60
A0602	21.18	5.32	3.30	—	—	-22.56	0.00	-22.56	—	0.47	0.17	0.23	58.0	41.3	-22.39
A0607	21.59	8.46	2.68	—	—	-23.26	0.00	-23.26	—	0.69	0.02	0.07	-60.2	31.1	-22.81
A0612	23.12	30.92	5.13	—	—	-24.96	0.00	-24.96	—	0.96	0.06	0.01	-81.9	4.2	-23.54
A0634	21.72	10.91	3.07	—	—	-23.22	0.00	-23.22	—	0.50	0.17	0.14	-77.2	67.5	-22.46
A0644	24.11	29.04	5.59	22.34	31.40	-23.64	-24.01	-24.59	0.71	0.85	0.23	0.49	7.4	10.4	-22.55
A0671	20.14	4.99	2.21	21.33	23.30	-23.23	-24.29	-24.64	0.38	0.73	0.21	0.27	23.7	30.7	-23.20
A0690	21.65	9.54	5.24	22.54	28.30	-23.72	-23.65	-24.44	1.06	0.66	0.10	0.20	41.7	53.0	-23.06
A0695	22.59	17.78	3.75	—	—	-23.90	0.00	-23.90	—	0.70	0.23	0.29	-53.4	-54.3	-22.79
A0744	24.10	40.05	6.33	—	—	-24.43	0.00	-24.43	—	0.76	0.03	0.06	71.6	-49.6	-22.86
A0757	20.80	4.44	2.17	23.23	23.50	-22.31	-22.42	-23.12	0.90	0.49	0.10	0.12	26.2	69.8	-22.23
A0779	20.70	7.99	3.72	21.60	27.20	-23.57	-23.97	-24.54	0.69	0.58	0.16	0.41	-23.7	-21.0	-23.10
A0780	21.94	10.39	3.70	22.30	26.25	-23.30	-23.60	-24.21	0.76	0.86	0.12	0.32	-36.5	-34.6	-22.85
A0819	24.42	57.38	6.85	—	—	-24.94	0.00	-24.94	—	0.71	0.25	0.45	-22.9	-27.4	-22.98
A0834	17.97	0.68	2.87	19.55	4.20	-21.21	-22.38	-22.70	0.34	0.47	0.36	0.27	-10.2	-5.7	-22.17
A0838	24.18	30.16	7.04	—	—	-23.70	0.00	-23.70	—	0.62	0.11	0.27	6.5	86.0	-22.39
A0841	21.15	7.34	4.35	22.88	33.50	-23.48	-23.61	-24.30	0.89	0.63	0.09	0.30	-29.8	-28.1	-22.95
A0865	21.03	3.79	1.17	—	—	-21.53	0.00	-21.53	—	0.23	0.45	0.51	-31.6	-29.9	-21.08
A0912	22.18	9.14	5.75	—	—	-23.03	0.00	-23.03	—	0.43	0.11	0.13	68.6	-9.1	-22.29
A0930	19.48	1.93	4.03	22.16	14.80	-22.14	-22.50	-23.09	0.72	0.58	0.08	0.18	-27.0	-8.2	-22.07
A0957	22.10	14.38	3.89	22.90	25.20	-23.89	-23.92	-24.66	0.97	0.86	0.20	0.22	-81.9	57.3	-23.00
A0970	21.81	6.50	5.24	23.01	23.90	-22.61	-22.70	-23.41	0.92	0.61	0.10	0.16	-54.6	-61.3	-22.19
A0978	20.74	5.67	5.21	21.91	23.70	-23.36	-23.76	-24.33	0.69	0.64	0.08	0.24	7.7	-18.1	-22.99
A0979	21.87	9.13	4.59	22.63	20.10	-23.19	-22.68	-23.71	1.60	0.65	0.07	0.11	-50.0	-39.3	-22.71
A0993	22.54	12.29	6.41	—	—	-23.35	0.00	-23.35	—	0.58	0.06	0.06	52.8	1.8	-23.05
A0994	22.61	18.69	4.90	—	—	-23.98	0.00	-23.98	—	0.54	0.35	0.41	-21.3	-18.6	-22.70
A0999	20.89	6.10	5.08	23.28	33.50	-23.15	-22.94	-23.80	1.22	0.44	0.19	0.24	-9.1	-29.4	-22.55
A1003	19.43	1.90	2.58	20.89	11.80	-21.96	-23.30	-23.58	0.29	0.70	0.06	0.29	-31.5	-53.8	-22.65
A1016	19.77	2.90	3.89	22.23	13.50	-22.52	-22.02	-23.05	1.59	0.43	0.10	0.14	9.6	0.1	-22.35
A1020	20.27	3.93	5.41	22.73	18.60	-23.10	-22.46	-23.58	1.79	0.53	0.05	0.16	-46.6	-41.8	-22.76
A1021	20.33	4.44	1.58	21.67	15.70	-22.82	-23.31	-23.84	0.64	0.64	0.17	0.25	-88.3	-89.8	-22.92
A1032	21.19	7.93	3.86	—	—	-23.52	0.00	-23.52	—	0.50	0.36	0.32	31.5	25.1	-22.59
A1035	23.46	28.91	5.38	—	—	-24.33	0.00	-24.33	—	0.73	0.06	0.15	-9.4	-14.6	-22.99

TABLE 2—*Continued*

Name (1)	$\mu_e$ (2)	$r_e$ (3)	$n$ (4)	$\mu_0$ (5)	$r_0$ (6)	$M_{Sersic}$ (7)	$M_{exp}$ (8)	$M_T$ (9)	$S/e$ (10)	$\alpha$ (11)	$e_{in}$ (12)	$e_{out}$ (13)	$pa_{in}$ (14)	$pa_{out}$ (15)	$M_{metric}$ (16)
A1066	20.73	6.52	2.26	23.01	47.10	-23.31	-24.22	-24.61	0.43	0.72	0.18	0.30	-40.4	-60.3	-22.84
A1069	21.28	6.61	5.03	21.20	16.30	-23.18	-23.71	-24.23	0.62	0.78	0.28	0.12	-86.8	-85.6	-22.98
A1100	20.49	4.99	2.33	21.97	20.90	-22.88	-23.39	-23.92	0.62	0.55	0.19	0.38	-10.0	-17.5	-22.74
A1139	21.39	6.74	4.83	22.45	22.60	-22.92	-22.99	-23.71	0.93	0.57	0.06	0.32	-51.2	-82.0	-22.55
A1142	22.65	15.08	6.67	23.46	49.00	-23.51	-23.60	-24.31	0.92	0.54	0.15	0.24	36.6	51.1	-22.55
A1145	21.49	6.31	3.56	—	—	-22.70	0.00	-22.70	—	0.44	0.17	0.16	-44.3	-50.1	-22.12
A1149	19.97	3.11	3.95	21.58	16.30	-22.74	-23.35	-23.84	0.57	0.65	0.11	0.33	68.8	69.7	-22.76
A1169	22.08	9.21	6.41	—	—	-23.21	0.00	-23.21	—	0.48	0.22	0.28	-32.0	-75.3	-22.25
A1171	20.03	3.54	2.62	22.42	22.00	-22.78	-23.18	-23.75	0.69	0.63	0.30	0.49	44.6	43.7	-22.26
A1177	23.13	20.88	6.41	22.29	29.00	-23.70	-23.62	-24.41	1.08	0.71	0.13	0.42	47.5	39.8	-22.77
A1185	21.45	10.10	1.87	23.94	95.70	-23.21	-24.60	-24.87	0.28	0.66	0.12	0.07	39.5	-15.0	-22.87
A1187	20.80	5.69	2.93	21.80	16.70	-23.14	-23.25	-23.95	0.91	0.64	0.18	0.21	-81.6	-65.2	-22.95
A1190	23.57	21.29	4.74	21.85	20.50	-23.48	-23.63	-24.31	0.87	0.95	0.28	0.32	-7.6	-12.4	-22.72
A1203	21.58	9.28	2.54	23.43	39.10	-23.33	-23.44	-24.14	0.90	0.75	0.16	0.17	-47.1	-25.8	-22.81
A1213	20.93	7.84	2.42	—	—	-23.41	0.00	-23.41	—	0.50	0.27	0.09	66.5	88.5	-22.75
A1216	19.77	2.69	1.85	21.22	9.80	-22.18	-22.54	-23.12	0.72	0.52	0.22	0.30	-50.2	-46.5	-22.38
A1228	19.39	2.34	4.18	21.81	12.10	-22.52	-22.25	-23.14	1.28	0.43	0.06	0.19	13.8	-42.3	-22.42
A1238	21.00	4.64	4.67	22.15	22.50	-22.67	-23.48	-23.90	0.47	0.68	0.08	0.43	-79.9	-77.7	-22.56
A1257	17.37	0.82	2.54	20.26	4.70	-21.97	-21.72	-22.61	1.26	0.24	0.10	0.13	-46.5	-43.0	-22.10
A1267	21.28	7.21	4.42	—	—	-23.05	0.00	-23.05	—	0.33	0.23	0.30	44.9	53.4	-22.43
A1270	20.34	6.21	1.59	—	—	-23.44	0.00	-23.44	—	0.48	0.43	0.20	-46.1	-45.3	-22.76
A1279	24.32	38.01	6.80	—	—	-24.07	0.00	-24.07	—	0.63	0.17	0.31	59.4	55.8	-22.56
A1308	21.99	9.41	4.13	23.29	34.60	-23.09	-23.20	-23.90	0.90	0.55	0.10	0.12	-26.0	-38.3	-22.61
A1314	19.76	3.67	2.54	21.67	23.70	-22.84	-23.82	-24.19	0.41	0.57	0.19	0.36	86.8	-86.2	-22.81
A1317	21.93	10.26	4.98	22.52	51.90	-23.50	-24.92	-25.18	0.27	0.73	0.18	0.57	38.9	55.4	-22.89
A1318	23.96	35.95	5.38	—	—	-24.18	0.00	-24.18	—	0.54	0.22	0.29	-8.8	-7.6	-22.75
A1334	21.66	8.47	5.05	—	—	-23.32	0.00	-23.32	—	0.51	0.21	0.22	88.8	77.4	-22.53
A1344	24.04	52.80	5.08	—	—	-24.98	0.00	-24.98	—	0.72	0.39	0.32	80.3	78.8	-23.05
A1365	22.79	15.86	6.62	—	—	-23.80	0.00	-23.80	—	0.50	0.21	0.22	-56.0	-62.1	-22.67
A1367	23.00	25.76	5.56	—	—	-23.97	0.00	-23.97	—	0.56	0.13	0.24	4.1	-10.8	-22.74
A1371	21.74	7.06	5.88	22.66	19.90	-22.99	-22.72	-23.62	1.28	0.65	0.08	0.19	59.6	44.0	-22.50
A1377	21.90	10.47	4.98	—	—	-23.50	0.00	-23.50	—	0.54	0.23	0.10	59.1	69.5	-22.66
A1400	23.35	22.75	3.34	—	—	-23.66	0.00	-23.66	—	0.81	0.16	0.23	-61.3	-65.9	-22.45
A1424	19.58	3.02	4.27	20.60	9.90	-23.17	-23.30	-23.99	0.89	0.63	0.25	0.15	72.4	70.3	-23.12
A1436	20.96	5.57	5.49	—	—	-23.21	0.00	-23.21	—	0.44	0.10	0.10	-79.8	-65.4	-22.56
A1452	23.87	34.05	6.85	—	—	-24.34	0.00	-24.34	—	0.66	0.08	0.12	48.0	52.9	-22.80
A1474	19.71	1.74	1.10	19.63	7.40	-21.20	-23.67	-23.78	0.10	0.67	0.51	0.58	-12.1	-10.0	-22.57
A1507	20.54	4.45	3.45	21.48	15.60	-22.88	-23.34	-23.89	0.65	0.70	0.20	0.29	48.0	44.1	-22.82
A1520	22.35	16.82	5.85	22.29	34.30	-24.23	-24.25	-24.99	0.98	0.75	0.16	0.33	-17.7	-32.1	-23.26
A1526	22.00	9.05	5.92	—	—	-23.29	0.00	-23.29	—	0.49	0.12	0.29	-88.4	-54.0	-22.39
A1534	20.75	6.44	3.46	22.32	20.90	-23.50	-23.17	-24.10	1.35	0.65	0.20	0.18	-48.9	-52.9	-23.01
A1569	19.78	3.06	3.17	20.37	11.00	-22.85	-23.77	-24.16	0.43	0.78	0.24	0.14	-74.2	-71.1	-23.19
A1589	24.90	76.44	8.20	—	—	-25.19	0.00	-25.19	—	0.73	0.25	0.41	73.4	65.8	-23.21
A1610	20.83	6.07	5.15	22.38	19.50	-23.46	-22.92	-23.98	1.65	0.55	0.09	0.25	-85.0	-68.0	-23.01
A1630	20.07	4.01	1.44	21.70	21.10	-22.66	-23.76	-24.10	0.36	0.61	0.23	0.37	83.1	86.4	-22.85
A1631	15.76	0.36	2.89	22.56	4.50	-22.00	-19.48	-22.10	10.17	0.67	0.12	0.12	19.0	18.6	-21.75
A1644	23.78	67.02	3.08	—	—	-25.38	0.00	-25.38	—	1.02	0.24	0.48	47.4	42.8	-23.00
A1648	20.47	4.95	0.96	21.81	24.20	-22.58	-24.01	-24.27	0.27	0.52	0.32	0.41	59.4	55.1	-22.78
A1691	22.55	22.89	2.99	—	—	-24.39	0.00	-24.39	—	0.92	0.18	0.07	-34.3	-14.1	-23.16
A1709	23.08	17.18	6.80	—	—	-23.57	0.00	-23.57	—	0.55	0.08	0.16	-53.0	-20.1	-22.63
A1736	23.34	39.24	6.21	—	—	-25.00	0.00	-25.00	—	0.58	0.33	0.43	-44.4	-45.1	-23.26
A1741	21.56	7.88	6.58	—	—	-23.49	0.00	-23.49	—	0.48	0.16	0.11	-34.9	-39.2	-22.69
A1749	20.41	5.81	3.27	22.04	22.40	-23.53	-23.54	-24.29	0.99	0.59	0.25	0.22	-85.8	-76.0	-23.10
A1767	25.23	101.01	6.02	—	—	-25.30	0.00	-25.30	—	0.81	0.09	0.39	-47.5	-3.6	-23.16
A1773	21.22	7.12	5.62	21.18	27.70	-23.52	-24.93	-25.19	0.27	0.65	0.27	0.07	30.0	12.5	-22.82
A1775	20.71	5.77	1.06	21.30	17.80	-22.70	-23.83	-24.16	0.35	0.85	0.12	0.16	-19.2	-28.6	-23.00
A1780	22.04	13.08	3.40	—	—	-23.75	0.00	-23.75	—	0.64	0.29	0.30	83.4	75.8	-22.70
A1795	20.94	6.02	1.88	21.70	27.50	-22.83	-24.37	-24.60	0.24	0.81	0.10	0.34	9.5	15.4	-22.94

TABLE 2—*Continued*

Name (1)	$\mu_e$ (2)	$r_e$ (3)	$n$ (4)	$\mu_0$ (5)	$r_0$ (6)	$M_{Sersic}$ (7)	$M_{exp}$ (8)	$M_T$ (9)	$S/e$ (10)	$\alpha$ (11)	$e_{in}$ (12)	$e_{out}$ (13)	$pa_{in}$ (14)	$pa_{out}$ (15)	$M_{metric}$ (16)
A1800	22.88	45.78	2.38	—	—	-25.46	0.00	-25.46	—	1.09	0.39	0.57	-18.6	-22.2	-23.23
A1809	21.78	12.38	4.93	22.81	45.50	-24.07	-24.37	-24.98	0.76	0.69	0.18	0.33	64.7	54.7	-23.26
A1825	22.29	10.97	4.90	23.24	27.90	-23.26	-22.84	-23.82	1.47	0.63	0.12	0.23	-15.0	-8.4	-22.60
A1827	22.01	10.76	6.06	—	—	-23.64	0.00	-23.64	—	0.57	0.15	0.07	36.0	54.2	-22.77
A1828	21.04	7.22	2.53	—	—	-23.28	0.00	-23.28	—	0.44	0.36	0.37	-33.6	-28.7	-22.53
A1831	22.75	18.26	4.98	21.80	28.20	-23.99	-24.37	-24.95	0.70	0.86	0.10	0.41	-20.0	-29.8	-23.23
A1836	23.22	26.32	5.24	—	—	-24.14	0.00	-24.14	—	0.60	0.09	0.29	48.6	37.8	-22.91
A1873	20.62	5.55	2.30	22.40	22.50	-23.07	-23.23	-23.90	0.87	0.60	0.13	0.26	-80.8	-87.1	-22.88
A1890	23.78	49.81	5.18	—	—	-25.08	0.00	-25.08	—	0.76	0.21	0.34	40.6	42.9	-23.26
A1898	23.37	18.80	6.13	—	—	-23.54	0.00	-23.54	—	0.60	0.11	0.17	1.9	21.2	-22.44
A1899	21.50	9.54	2.83	—	—	-23.41	0.00	-23.41	—	0.58	0.36	0.33	-43.1	82.3	-22.59
A1904	21.91	12.00	4.76	21.85	22.30	-23.88	-23.80	-24.59	1.08	0.76	0.17	0.35	20.9	44.4	-23.18
A1913	21.99	10.73	6.02	—	—	-23.55	0.00	-23.55	—	0.56	0.04	0.00	24.3	-72.1	-22.76
A1964	19.74	2.78	5.29	22.10	23.00	-22.89	-23.58	-24.04	0.53	0.57	0.16	0.10	14.6	-24.2	-22.52
A1982	20.94	5.80	3.09	21.44	16.10	-22.96	-23.42	-23.96	0.65	0.67	0.30	0.40	48.3	46.9	-22.72
A1983	21.89	11.28	6.29	—	—	-23.76	0.00	-23.76	—	0.34	0.26	0.29	28.4	26.9	-22.59
A1991	26.26	201.64	6.41	—	—	-25.74	0.00	-25.74	—	0.90	0.18	0.36	15.6	9.7	-22.86
A2020	19.37	1.43	4.08	19.76	4.70	-21.59	-22.38	-22.81	0.49	0.46	0.48	0.44	-35.5	-35.4	-21.96
A2022	19.94	3.62	3.55	21.98	22.70	-22.99	-23.61	-24.10	0.57	0.65	0.12	0.12	-34.2	-56.8	-22.88
A2025	19.89	4.84	2.07	21.90	22.30	-23.61	-23.86	-24.49	0.79	0.56	0.21	0.06	-51.1	-45.9	-23.44
A2028	21.57	10.27	3.32	22.78	35.40	-23.68	-23.86	-24.52	0.84	0.71	0.20	0.32	-81.1	-81.4	-23.05
A2029	26.30	439.41	5.78	—	—	-27.40	0.00	-27.40	—	1.05	0.26	0.52	20.5	26.6	-23.58
A2040	20.57	3.67	5.21	21.94	26.20	-22.54	-23.90	-24.17	0.28	0.72	0.12	0.44	-55.2	-55.8	-22.43
A2052	24.76	73.57	3.89	—	—	-24.58	0.00	-24.58	—	0.88	0.16	0.35	34.6	35.5	-22.56
A2055	21.19	5.15	3.80	21.86	21.00	-22.51	-23.52	-23.88	0.39	0.42	0.25	0.35	-26.1	27.1	-21.89
A2063	24.15	44.25	4.27	—	—	-24.21	0.00	-24.21	—	0.80	0.04	0.38	39.0	29.1	-22.71
A2065	23.87	27.62	7.30	—	—	-23.90	0.00	-23.90	—	0.67	0.18	0.09	2.9	11.1	-22.51
A2107	23.19	35.86	3.68	—	—	-24.64	0.00	-24.64	—	0.79	0.13	0.26	-71.3	-63.5	-23.09
A2143	21.06	5.41	6.21	21.87	15.10	-23.20	-22.99	-23.85	1.21	0.72	0.06	0.08	21.1	16.3	-22.84
A2147	22.28	14.87	3.23	23.15	78.10	-23.58	-25.04	-25.29	0.26	0.81	0.23	0.64	12.8	11.9	-22.68
A2152	21.86	9.98	6.45	—	—	-23.53	0.00	-23.53	—	0.48	0.07	0.08	16.4	-70.5	-22.68
A2162	20.85	7.19	3.92	22.46	28.20	-23.40	-23.38	-24.14	1.02	0.57	0.24	0.36	5.1	1.0	-22.81
A2184	21.65	7.05	3.19	—	—	-22.66	0.00	-22.66	—	0.49	0.15	0.26	-15.0	-17.7	-22.17
A2197	19.25	3.71	1.54	20.32	13.50	-23.05	-23.88	-24.29	0.47	0.60	0.29	0.37	-39.7	-35.3	-23.24
A2198	21.42	5.64	5.00	—	—	-22.66	0.00	-22.66	—	0.42	0.12	0.20	-8.2	-3.6	-21.98
A2199	21.18	7.95	1.40	21.82	26.90	-22.76	-23.91	-24.23	0.35	0.81	0.15	0.36	27.1	33.3	-22.81
A2247	21.13	6.67	2.19	—	—	-22.73	0.00	-22.73	—	0.41	0.10	0.23	27.2	3.4	-22.34
A2248	22.53	13.34	6.41	—	—	-23.56	0.00	-23.56	—	0.56	0.07	0.19	14.9	13.0	-22.66
A2250	21.28	7.12	4.02	—	—	-23.22	0.00	-23.22	—	0.44	0.16	0.10	-36.6	-74.4	-22.59
A2256	20.84	8.91	1.87	—	—	-23.73	0.00	-23.73	—	0.52	0.35	0.30	-80.6	-76.1	-22.97
A2271	23.96	52.68	3.86	—	—	-24.86	0.00	-24.86	—	0.90	0.21	0.37	-57.8	-53.3	-22.94
A2293	23.19	19.05	5.99	—	—	-23.68	0.00	-23.68	—	0.73	0.26	0.33	76.8	72.4	-22.61
A2296	19.63	1.42	4.35	21.02	8.60	-21.31	-22.39	-22.73	0.37	0.60	0.19	0.40	68.1	72.4	-21.72
A2308	24.51	44.68	6.37	—	—	-24.28	0.00	-24.28	—	0.74	0.07	0.26	38.5	17.9	-22.73
A2309	20.02	3.49	4.18	22.17	17.80	-22.88	-22.86	-23.62	1.02	0.57	0.21	0.22	-61.2	-68.0	-22.67
A2319	25.16	71.27	5.00	21.19	17.60	-24.40	-23.83	-24.91	1.69	1.12	0.15	0.18	4.4	20.1	-22.99
A2331	22.07	6.98	5.18	21.67	17.50	-22.57	-23.44	-23.84	0.45	0.86	0.06	0.27	-86.3	89.4	-22.59
A2361	22.83	15.13	7.14	—	—	-23.58	0.00	-23.58	—	0.52	0.07	0.16	50.6	49.7	-22.67
A2362	22.52	15.75	6.13	—	—	-23.91	0.00	-23.91	—	0.55	0.15	0.09	68.6	85.0	-23.01
A2366	19.64	3.60	1.64	21.32	16.50	-22.87	-23.56	-24.02	0.53	0.59	0.14	0.15	-30.6	-21.7	-23.08
A2372	20.16	4.35	1.55	21.97	17.40	-22.75	-23.05	-23.66	0.76	0.58	0.13	0.29	7.2	-4.4	-22.81
A2381	17.19	0.43	4.10	20.31	3.20	-20.86	-20.70	-21.54	1.15	0.22	0.22	0.35	6.1	4.8	-21.03
A2382	20.41	3.97	1.55	21.31	16.30	-22.33	-23.59	-23.89	0.31	0.82	0.17	0.10	8.6	-67.8	-22.76
A2383	21.35	5.54	3.64	—	—	-22.62	0.00	-22.62	—	0.36	0.33	0.36	-47.7	-49.8	-21.98
A2388	25.06	57.29	6.71	—	—	-24.22	0.00	-24.22	—	0.68	0.13	0.44	-80.5	-75.2	-22.46
A2399	21.75	12.37	3.91	—	—	-23.91	0.00	-23.91	—	0.62	0.32	0.21	-77.3	-70.1	-22.92
A2401	23.47	26.80	6.99	—	—	-24.16	0.00	-24.16	—	0.67	0.07	0.17	-12.2	-34.9	-23.03
A2412	20.33	4.55	1.79	23.43	90.80	-22.81	-25.23	-25.34	0.11	0.57	0.15	0.11	31.0	22.6	-22.65

TABLE 2—*Continued*

Name (1)	$\mu_e$ (2)	$r_e$ (3)	$n$ (4)	$\mu_0$ (5)	$r_0$ (6)	$M_{Sersic}$ (7)	$M_{exp}$ (8)	$M_T$ (9)	$S/e$ (10)	$\alpha$ (11)	$e_{in}$ (12)	$e_{out}$ (13)	$pa_{in}$ (14)	$pa_{out}$ (15)	$M_{metric}$ (16)
A2415	23.75	31.01	6.94	—	—	-24.20	0.00	-24.20	—	0.60	0.21	0.35	27.1	25.5	-22.76
A2457	21.10	8.46	2.60	22.33	31.60	-23.52	-23.98	-24.52	0.65	0.73	0.26	0.41	86.2	83.0	-23.06
A2459	21.25	8.03	2.36	—	—	-23.25	0.00	-23.25	—	0.49	0.28	0.26	13.2	3.0	-22.68
A2462	20.29	4.35	5.13	22.37	26.20	-23.40	-23.70	-24.32	0.76	0.61	0.03	0.26	-89.8	-52.5	-23.05
A2480	19.86	3.45	3.82	22.23	22.80	-23.16	-23.51	-24.10	0.72	0.51	0.03	0.48	-18.0	-40.0	-23.00
A2492	20.93	5.61	2.81	22.25	18.50	-22.98	-23.04	-23.76	0.95	0.63	0.13	0.29	-70.0	89.6	-22.80
A2495	21.70	6.56	1.30	21.52	26.60	-22.20	-24.59	-24.71	0.11	1.01	0.18	0.43	50.4	50.7	-22.70
A2511	21.60	7.66	2.83	—	—	-22.92	0.00	-22.92	—	0.49	0.22	0.22	81.3	75.1	-22.31
A2524	21.19	7.10	4.65	22.03	17.90	-23.44	-23.14	-24.05	1.33	0.63	0.19	0.28	14.5	1.9	-22.93
A2525	20.52	3.78	4.31	23.00	22.60	-22.69	-22.66	-23.43	1.03	0.56	0.07	0.16	-61.4	-48.7	-22.35
A2559	23.97	36.62	5.18	21.65	22.80	-24.28	-24.04	-24.91	1.25	0.86	0.29	0.53	29.7	31.8	-23.01
A2572	19.18	2.54	1.37	21.31	17.30	-22.43	-23.62	-23.93	0.34	0.50	0.23	0.18	-85.8	-19.2	-22.81
A2589	28.54	725.91	9.52	—	—	-26.43	0.00	-26.43	—	0.78	0.12	0.51	-11.1	5.0	-22.96
A2593	21.93	6.60	4.83	20.54	12.00	-22.40	-23.65	-23.95	0.33	0.90	0.18	0.38	75.2	73.8	-22.44
A2596	19.91	2.30	1.02	20.50	6.10	-21.62	-22.44	-22.86	0.47	0.55	0.05	0.16	-76.0	-70.8	-22.47
A2618	20.79	6.60	1.69	21.94	25.50	-23.11	-23.95	-24.36	0.46	0.80	0.06	0.26	77.2	-86.4	-23.15
A2622	24.53	51.76	6.13	—	—	-24.49	0.00	-24.49	—	0.78	0.20	0.42	-43.3	-55.4	-22.78
A2625	21.60	10.49	3.10	—	—	-23.67	0.00	-23.67	—	0.54	0.37	0.36	84.9	85.9	-22.78
A2626	24.10	37.52	4.48	21.48	17.00	-24.14	-23.58	-24.65	1.67	1.05	0.24	0.37	32.3	32.0	-22.92
A2630	22.56	15.00	5.56	—	—	-23.83	0.00	-23.83	—	0.59	0.05	0.31	-49.4	-50.5	-22.87
A2634	20.33	4.66	3.16	21.27	20.60	-22.98	-24.00	-24.35	0.39	0.67	0.18	0.45	31.0	34.3	-22.98
A2637	23.01	22.64	6.58	—	—	-24.38	0.00	-24.38	—	0.58	0.21	0.37	62.9	86.1	-23.17
A2644	23.31	22.24	5.46	—	—	-23.94	0.00	-23.94	—	0.57	0.19	0.30	16.9	28.3	-22.73
A2656	20.46	3.20	4.29	21.22	13.20	-22.48	-23.37	-23.76	0.44	0.81	0.09	0.22	-27.1	-8.4	-22.81
A2657	21.24	2.74	3.94	19.76	3.50	-21.04	-21.67	-22.15	0.56	0.36	0.11	0.07	1.8	-9.3	-21.95
A2660	22.08	10.53	5.62	22.42	20.60	-23.40	-22.94	-23.95	1.53	0.63	0.25	0.45	-35.3	-27.8	-22.65
A2661	26.51	104.60	6.13	—	—	-24.53	0.00	-24.53	—	0.92	0.28	0.30	-76.0	-36.4	-22.27
A2665	23.94	50.12	4.15	—	—	-24.77	0.00	-24.77	—	0.93	0.13	0.32	-64.7	-80.7	-23.00
A2666	22.97	25.07	6.37	—	—	-24.34	0.00	-24.34	—	0.61	0.26	0.32	60.6	60.7	-23.05
A2670	21.13	7.49	5.43	21.75	22.30	-23.69	-23.88	-24.54	0.84	0.70	0.09	0.08	81.4	-39.7	-23.28
A2675	24.31	40.53	6.45	—	—	-24.24	0.00	-24.24	—	0.71	0.09	0.44	43.8	45.0	-22.78
A2678	21.85	8.54	6.41	—	—	-23.32	0.00	-23.32	—	0.48	0.18	0.23	17.7	19.0	-22.55
A2716	20.71	5.35	6.45	—	—	-23.43	0.00	-23.43	—	0.43	0.21	0.17	-78.3	-81.0	-22.66
A2717	20.15	2.80	2.84	21.25	18.60	-22.08	-23.88	-24.07	0.19	0.87	0.05	0.18	-17.3	8.3	-22.64
A2731	22.31	16.35	6.62	—	—	-24.12	0.00	-24.12	—	0.55	0.36	0.23	88.0	77.0	-22.76
A2734	21.70	9.87	1.27	22.08	32.30	-22.91	-24.29	-24.56	0.28	1.03	0.19	0.50	21.5	21.6	-22.76
A2764	22.17	14.97	5.43	—	—	-24.13	0.00	-24.13	—	0.60	0.16	0.18	-37.4	1.5	-23.06
A2765	19.33	2.05	4.59	21.75	9.30	-22.58	-21.98	-23.08	1.74	0.54	0.24	0.29	51.7	51.8	-22.09
A2799	22.79	16.32	6.10	—	—	-23.73	0.00	-23.73	—	0.63	0.22	0.25	42.8	32.0	-22.54
A2800	22.38	14.39	4.42	—	—	-23.70	0.00	-23.70	—	0.62	0.25	0.42	63.4	75.7	-22.71
A2806	19.85	3.12	3.32	21.11	7.20	-22.59	-21.86	-23.04	1.97	0.46	0.16	0.20	-62.5	-58.7	-22.60
A2814	22.20	12.53	5.10	—	—	-23.73	0.00	-23.73	—	0.59	0.21	0.26	-34.6	-31.0	-22.78
A2819	20.27	5.19	2.62	—	—	-23.36	0.00	-23.36	—	0.63	0.24	0.18	42.4	35.2	-22.62
A2824	21.68	7.93	5.26	—	—	-23.29	0.00	-23.29	—	0.45	0.14	0.03	65.4	30.1	-22.51
A2836	21.80	6.84	2.75	—	—	-22.46	0.00	-22.46	—	0.49	0.07	0.10	-53.4	-37.0	-22.12
A2841	21.11	7.02	4.93	22.16	20.23	-23.46	-23.21	-24.10	1.26	0.63	0.26	0.36	-14.2	-10.8	-22.87
A2854	21.39	4.80	5.59	22.11	24.50	-22.41	-23.66	-23.96	0.32	0.65	0.18	0.50	-2.6	-15.7	-22.28
A2859	20.74	4.48	5.29	22.48	15.90	-22.91	-22.37	-23.43	1.64	0.53	0.15	0.23	-89.4	-77.9	-22.92
A2864	18.86	1.55	5.08	21.75	10.20	-22.48	-22.16	-23.08	1.34	0.55	0.17	0.26	28.6	34.4	-22.17
A2870	22.96	22.83	4.63	—	—	-23.97	0.00	-23.97	—	0.70	0.27	0.24	10.5	11.6	-22.72
A2877	19.91	5.63	3.68	21.04	19.90	-23.63	-23.89	-24.52	0.78	0.68	0.14	0.28	-69.5	-92.9	-23.44
A2881	19.41	2.00	2.67	21.66	8.70	-22.12	-21.88	-22.76	1.26	0.46	0.16	0.15	46.4	65.0	-22.22
A2889	19.88	1.44	1.01	22.05	5.70	-20.29	-20.41	-21.10	0.90	0.34	0.42	0.38	-44.4	-41.4	-20.49
A2896	18.95	2.21	3.68	21.01	8.50	-22.71	-22.23	-23.25	1.56	0.40	0.27	0.33	-62.6	-65.8	-22.44
A2911	19.64	2.34	2.82	22.01	11.90	-21.72	-21.67	-22.45	1.04	0.47	0.17	0.23	-18.4	14.5	-21.78
A2923	22.24	13.42	4.15	—	—	-23.69	0.00	-23.69	—	0.66	0.03	0.29	66.1	75.8	-22.89
A2954	20.76	3.80	1.68	—	—	-22.04	0.00	-22.04	—	0.32	0.18	0.26	27.3	33.6	-21.73
A2955	19.71	2.58	5.21	21.53	19.00	-22.92	-23.89	-24.27	0.41	0.74	0.11	0.49	78.6	67.6	-22.84

TABLE 2—*Continued*

Name (1)	$\mu_e$ (2)	$r_e$ (3)	$n$ (4)	$\mu_0$ (5)	$r_0$ (6)	$M_{Sersic}$ (7)	$M_{exp}$ (8)	$M_T$ (9)	$S/e$ (10)	$\alpha$ (11)	$e_{in}$ (12)	$e_{out}$ (13)	$pa_{in}$ (14)	$pa_{out}$ (15)	$M_{metric}$ (16)
A2992	21.38	7.57	4.69	—	—	-23.31	0.00	-23.31	—	0.43	0.29	0.30	-59.6	-53.9	-22.51
A3004	22.51	13.82	5.24	—	—	-23.58	0.00	-23.58	—	0.63	0.12	0.13	-54.9	37.2	-22.59
A3009	23.29	32.22	3.58	—	—	-24.43	0.00	-24.43	—	0.88	0.16	0.44	-71.3	-74.5	-23.02
A3027	23.36	20.33	5.75	23.01	32.60	-23.67	-23.46	-24.32	1.22	0.69	0.26	0.38	84.0	85.7	-22.62
A3047	21.99	8.22	4.55	21.93	23.03	-23.01	-23.84	-24.26	0.46	0.81	0.22	0.45	-59.4	-48.3	-22.80
A3074	23.73	45.61	4.33	—	—	-24.88	0.00	-24.88	—	0.84	0.32	0.43	35.2	33.8	-23.04
A3077	22.53	11.53	4.55	—	—	-23.17	0.00	-23.17	—	0.50	0.46	0.49	74.3	67.3	-22.08
A3078	23.86	38.66	4.83	—	—	-24.45	0.00	-24.45	—	0.81	0.16	0.32	30.6	16.0	-22.90
A3089	20.44	3.42	4.65	21.50	10.40	-22.55	-22.43	-23.24	1.12	0.61	0.17	0.29	76.4	79.6	-22.41
A3093	22.00	10.57	3.44	21.64	18.40	-23.34	-23.60	-24.23	0.79	0.81	0.28	0.46	20.3	18.8	-22.89
A3094	22.38	15.17	5.24	—	—	-23.92	0.00	-23.92	—	0.69	0.16	0.17	34.3	52.3	-22.84
A3095	19.63	2.88	3.11	21.50	11.20	-22.77	-22.59	-23.43	1.18	0.48	0.15	0.31	-5.3	-16.0	-22.75
A3098	26.40	186.16	6.90	—	—	-25.55	0.00	-25.55	—	0.84	0.24	0.48	-40.0	-39.4	-22.80
A3100	21.92	10.00	2.11	—	—	-22.97	0.00	-22.97	—	0.73	0.32	0.14	67.0	70.4	-22.33
A3104	18.96	2.03	3.22	21.38	21.04	-22.73	-24.11	-24.38	0.28	0.66	0.25	0.45	63.0	68.7	-22.77
A3107	20.72	4.07	3.28	22.92	25.49	-22.47	-22.96	-23.50	0.63	0.54	0.19	0.18	-30.2	-44.7	-22.21
A3108	22.79	12.73	4.67	—	—	-23.04	0.00	-23.04	—	0.58	0.25	0.36	70.5	65.7	-22.08
A3109	24.03	47.17	6.41	—	—	-24.81	0.00	-24.81	—	0.71	0.33	0.16	16.0	22.2	-22.89
A3110	20.30	6.54	1.89	20.87	12.80	-23.67	-23.55	-24.36	1.11	0.61	0.50	0.39	-2.1	-2.1	-23.21
A3111	21.72	7.84	5.18	21.70	16.70	-23.18	-23.31	-24.00	0.89	0.75	0.12	0.14	33.2	62.9	-22.87
A3112	24.95	71.55	6.54	22.01	33.50	-24.87	-24.50	-25.45	1.40	0.88	0.33	0.59	9.2	6.7	-23.06
A3120	21.67	8.16	4.18	22.01	24.50	-23.03	-23.67	-24.15	0.56	0.79	0.27	0.48	-26.5	-37.1	-22.57
A3122	20.51	5.83	5.78	22.82	27.10	-23.76	-23.20	-24.27	1.68	0.60	0.27	0.39	38.0	61.4	-22.96
A3123	18.69	1.70	3.60	20.69	8.10	-22.63	-22.68	-23.41	0.95	0.54	0.33	0.34	-81.9	-64.7	-22.65
A3125	19.83	2.86	3.04	21.83	9.70	-22.52	-21.92	-23.01	1.73	0.49	0.07	0.13	-2.9	-34.0	-22.46
A3128	23.58	32.96	6.10	—	—	-24.45	0.00	-24.45	—	0.67	0.19	0.20	11.3	25.5	-22.99
A3133	24.37	25.14	6.80	—	—	-23.18	0.00	-23.18	—	0.59	0.25	0.36	-26.8	-29.0	-21.82
A3135	22.71	14.77	5.88	—	—	-23.56	0.00	-23.56	—	0.56	0.13	0.27	33.2	51.3	-22.57
A3142	20.80	5.23	3.32	21.92	17.64	-22.94	-23.16	-23.81	0.81	0.64	0.21	0.30	-12.1	-21.4	-22.71
A3144	22.52	11.20	7.35	—	—	-23.20	0.00	-23.20	—	0.48	0.14	0.12	-69.1	-26.7	-22.38
A3151	18.38	1.22	2.70	21.27	11.10	-22.09	-22.81	-23.27	0.52	0.70	0.09	0.28	-67.3	-17.0	-22.33
A3152	23.10	20.44	6.29	—	—	-24.05	0.00	-24.05	—	0.56	0.32	0.34	0.9	2.6	-22.59
A3153	23.84	25.55	5.78	—	—	-23.85	0.00	-23.85	—	0.71	0.16	0.39	87.1	92.6	-22.56
A3158	23.45	30.76	6.02	—	—	-24.43	0.00	-24.43	—	0.73	0.11	0.14	63.3	59.7	-23.06
A3164	23.18	20.63	7.04	—	—	-23.91	0.00	-23.91	—	0.59	0.10	0.20	-59.8	30.3	-22.94
A3188	19.77	2.00	6.02	—	—	-22.19	0.00	-22.19	—	0.32	0.20	0.28	-50.7	-66.8	-21.40
A3193	23.10	19.45	6.49	—	—	-23.72	0.00	-23.72	—	0.54	0.10	0.24	-82.5	87.3	-22.57
A3195	23.28	22.96	5.99	—	—	-24.02	0.00	-24.02	—	0.67	0.32	0.39	64.0	60.6	-22.72
A3223	20.01	4.49	1.84	21.61	16.00	-23.06	-23.23	-23.90	0.85	0.56	0.26	0.26	0.6	-6.8	-22.98
A3225	19.61	2.40	0.93	20.28	7.50	-21.74	-22.88	-23.21	0.35	0.64	0.13	0.16	-11.3	-8.0	-22.68
A3229	20.06	2.40	2.07	—	—	-21.54	0.00	-21.54	—	0.24	0.46	0.48	-78.7	-85.9	-21.07
A3231	22.28	7.98	5.56	—	—	-22.69	0.00	-22.69	—	0.49	0.07	0.15	84.4	84.5	-21.90
A3234	21.60	7.72	4.93	—	—	-23.41	0.00	-23.41	—	0.49	0.20	0.13	27.9	33.3	-22.55
A3266	20.23	4.04	5.59	21.02	26.10	-23.20	-24.89	-25.09	0.21	0.83	0.12	0.31	77.4	63.4	-23.19
A3301	21.83	13.08	3.11	23.26	80.22	-23.81	-25.06	-25.36	0.32	0.81	0.07	0.37	-45.8	-42.7	-23.15
A3332	20.94	5.94	4.12	23.16	36.36	-23.24	-23.55	-24.16	0.75	0.52	0.12	0.44	48.5	47.7	-22.83
A3336	22.95	20.24	4.12	23.28	42.50	-23.90	-23.77	-24.59	1.12	0.82	0.22	0.34	19.5	17.8	-22.82
A3341	21.09	4.95	6.06	21.71	16.80	-22.72	-23.14	-23.70	0.68	0.72	0.21	0.33	11.8	21.7	-22.44
A3351	21.63	7.82	6.25	—	—	-23.43	0.00	-23.43	—	0.52	0.10	0.06	-34.1	71.5	-22.58
A3354	20.15	3.80	2.38	22.75	22.40	-22.69	-22.82	-23.51	0.89	0.47	0.09	0.15	3.9	1.2	-22.63
A3367	21.91	10.08	3.46	—	—	-23.19	0.00	-23.19	—	0.39	0.27	0.35	52.1	54.9	-22.24
A3374	14.82	0.24	2.79	19.08	4.00	-22.02	-22.67	-23.14	0.55	0.46	0.44	0.40	-70.5	-70.6	-22.17
A3376	20.91	7.24	2.87	22.28	30.50	-23.37	-23.91	-24.43	0.61	0.68	0.28	0.44	64.4	67.9	-22.87
A3380	21.71	7.91	5.38	23.40	56.80	-23.12	-24.16	-24.51	0.38	0.58	0.07	0.41	81.2	69.2	-22.56
A3381	24.08	29.06	6.45	—	—	-23.60	0.00	-23.60	—	0.64	0.11	0.18	36.0	29.9	-22.28
A3389	21.84	13.47	3.07	—	—	-23.77	0.00	-23.77	—	0.69	0.18	0.16	60.3	19.8	-22.88
A3390	21.20	5.15	5.65	21.91	15.90	-22.66	-22.83	-23.50	0.86	0.65	0.04	0.12	-79.5	-75.0	-22.55
A3391	22.44	22.42	3.31	—	—	-24.41	0.00	-24.41	—	0.74	0.24	0.38	76.1	45.6	-23.15

TABLE 2—*Continued*

Name (1)	$\mu_e$ (2)	$r_e$ (3)	$n$ (4)	$\mu_0$ (5)	$r_0$ (6)	$M_{Sersic}$ (7)	$M_{exp}$ (8)	$M_T$ (9)	$S/e$ (10)	$\alpha$ (11)	$e_{in}$ (12)	$e_{out}$ (13)	$pa_{in}$ (14)	$pa_{out}$ (15)	$M_{metric}$ (16)
A3395	26.19	202.47	5.78	—	—	-25.71	0.00	-25.71	—	0.88	0.38	0.57	-56.2	-63.4	-22.56
A3404	24.18	56.46	3.28	—	—	-25.09	0.00	-25.09	—	1.14	0.29	0.39	66.6	70.6	-22.94
A3407	25.64	99.66	7.87	—	—	-24.90	0.00	-24.90	—	0.74	0.08	0.02	-88.9	34.5	-22.84
A3408	22.46	16.24	5.78	23.25	46.90	-23.93	-23.85	-24.64	1.07	0.64	0.08	0.33	-43.7	-39.8	-23.02
A3420	20.70	4.42	4.85	23.22	19.60	-22.86	-22.08	-23.29	2.06	0.44	0.20	0.22	38.7	38.8	-22.42
A3429	24.66	53.10	7.04	—	—	-24.43	0.00	-24.43	—	0.70	0.21	0.47	39.7	38.8	-22.67
A3490	21.28	6.22	4.81	22.69	26.70	-23.17	-23.43	-24.06	0.79	0.67	0.13	0.26	37.5	57.1	-22.73
A3497	24.02	32.71	5.46	—	—	-23.97	0.00	-23.97	—	0.75	0.18	0.29	50.6	43.8	-22.47
A3528	22.24	14.03	5.15	22.33	36.20	-23.91	-24.36	-24.91	0.66	0.68	0.17	0.47	0.2	-5.8	-23.16
A3530	22.94	17.98	5.71	21.47	25.30	-23.80	-24.43	-24.91	0.56	0.80	0.23	0.45	-54.7	-34.6	-23.05
A3531	22.03	4.76	6.10	21.98	17.50	-21.76	-23.02	-23.31	0.31	0.85	0.37	0.51	15.9	15.3	-21.71
A3532	22.33	11.85	5.65	22.40	42.40	-23.51	-24.64	-24.97	0.36	0.76	0.15	0.39	64.5	79.2	-22.89
A3537	22.17	17.15	5.52	—	—	-23.84	0.00	-23.84	—	0.57	0.31	0.27	-12.5	-26.0	-22.70
A3549	21.91	8.42	5.26	—	—	-23.05	0.00	-23.05	—	0.45	0.29	0.26	3.1	3.0	-22.14
A3549	23.03	11.69	5.81	—	—	-22.78	0.00	-22.78	—	0.58	0.10	0.09	-68.2	69.6	-21.95
A3552	22.27	20.56	6.02	—	—	-24.70	0.00	-24.70	—	0.60	0.08	0.06	22.3	87.4	-22.58
A3553	22.33	9.53	4.00	—	—	-22.81	0.00	-22.81	—	0.56	0.04	0.09	-88.9	47.3	-22.22
A3554	23.55	20.03	5.78	21.46	20.20	-23.39	-23.91	-24.43	0.62	0.82	0.24	0.34	-35.6	-49.2	-22.68
A3556	22.15	18.39	4.05	—	—	-24.42	0.00	-24.42	—	0.68	0.32	0.14	-35.9	-40.1	-23.18
A3559	24.73	112.07	4.63	—	—	-25.76	0.00	-25.76	—	0.99	0.13	0.35	-22.8	-21.0	-23.26
A3559	18.15	1.61	4.88	20.60	14.10	-23.22	-23.98	-24.42	0.50	0.61	0.19	0.42	28.4	47.3	-23.18
A3560	20.62	5.86	3.57	—	—	-22.54	0.00	-22.54	—	0.46	0.21	0.07	72.8	-45.3	-22.11
A3562	22.28	15.39	2.92	22.96	72.90	-23.74	-25.21	-25.46	0.26	0.80	0.20	0.57	89.7	84.0	-22.88
A3564	21.93	7.10	5.78	—	—	-22.78	0.00	-22.78	—	0.43	0.13	0.05	-50.0	-41.9	-22.20
A3564	21.95	10.15	4.13	—	—	-23.35	0.00	-23.35	—	0.54	0.14	0.11	-0.8	-12.5	-22.62
A3565	23.47	36.59	7.75	—	—	-24.10	0.00	-24.10	—	0.64	0.09	0.05	60.3	8.7	-22.76
A3570	20.62	4.88	4.22	—	—	-22.99	0.00	-22.99	—	0.39	0.15	0.12	5.2	73.2	-22.50
A3571	25.51	232.87	4.57	—	—	-26.54	0.00	-26.54	—	1.16	0.24	0.64	1.7	3.8	-23.14
A3572	21.12	6.30	5.68	—	—	-23.22	0.00	-23.22	—	0.40	0.07	0.12	30.0	-64.2	-22.61
A3574	22.15	11.42	6.17	20.69	17.80	-22.94	-23.74	-24.17	0.48	0.76	0.14	0.45	68.6	67.2	-22.64
A3575	20.94	3.70	5.99	—	—	-22.24	0.00	-22.24	—	0.32	0.07	0.13	-66.8	-63.9	-21.78
A3581	25.38	74.80	8.20	—	—	-24.22	0.00	-24.22	—	0.65	0.13	0.34	-65.4	-70.8	-22.41
A3605	21.58	10.17	1.46	23.35	56.40	-23.20	-24.27	-24.62	0.37	0.90	0.10	0.22	59.0	51.9	-22.80
A3626	22.10	10.36	1.05	—	—	-22.55	0.00	-22.55	—	0.78	0.31	0.41	19.5	32.7	-21.97
A3631	21.57	6.64	0.81	—	—	-22.01	0.00	-22.01	—	0.49	0.31	0.25	-50.9	-52.7	-21.66
A3651	22.29	19.27	2.46	—	—	-24.10	0.00	-24.10	—	0.91	0.13	0.19	-34.1	-34.8	-23.08
A3656	24.07	41.74	8.00	—	—	-24.45	0.00	-24.45	—	0.61	0.17	0.18	-55.5	-67.1	-22.84
A3667	20.88	7.19	1.47	22.01	32.00	-23.09	-24.32	-24.62	0.32	0.90	0.17	0.36	67.9	-46.1	-23.03
A3677	22.02	8.90	4.78	—	—	-22.96	0.00	-22.96	—	0.47	0.23	0.31	-45.7	-42.1	-22.11
A3687	25.22	71.69	6.99	—	—	-24.63	0.00	-24.63	—	0.72	0.22	0.38	-46.5	-44.2	-22.57
A3698	21.89	10.61	6.37	—	—	-23.16	0.00	-23.16	—	0.42	0.31	0.44	8.4	5.4	-22.13
A3703	23.23	19.73	6.13	23.09	41.10	-23.73	-23.84	-24.54	0.90	0.70	0.22	0.47	-87.8	79.9	-22.59
A3716	22.34	11.69	5.88	21.57	20.00	-23.39	-23.74	-24.33	0.73	0.78	0.05	0.32	63.5	56.7	-22.91
A3731	20.21	4.32	3.04	22.32	23.17	-22.99	-23.28	-23.90	0.77	0.56	0.11	0.30	-13.0	-0.3	-22.80
A3733	20.21	2.79	1.22	21.23	11.40	-21.47	-22.71	-23.01	0.32	0.64	0.13	0.20	7.3	-2.2	-22.16
A3736	24.14	65.96	5.85	—	—	-25.33	0.00	-25.33	—	0.79	0.31	0.48	24.4	23.9	-23.24
A3742	21.57	8.81	7.04	—	—	-23.01	0.00	-23.01	—	0.45	0.28	0.14	-46.5	-39.1	-22.15
A3744	22.33	12.68	6.37	—	—	-23.48	0.00	-23.48	—	0.55	0.02	0.11	39.8	12.8	-22.65
A3747	22.21	13.72	4.35	—	—	-23.61	0.00	-23.61	—	0.54	0.35	0.41	38.7	25.9	-22.52
A3756	22.03	10.94	5.18	—	—	-23.49	0.00	-23.49	—	0.50	0.22	0.31	-37.2	-43.4	-22.60
A3764	22.36	12.13	6.25	—	—	-23.60	0.00	-23.60	—	0.56	0.12	0.23	-68.2	-31.7	-22.70
A3771	19.25	2.00	2.44	21.84	14.90	-22.28	-22.92	-23.40	0.56	0.58	0.16	0.26	21.6	10.3	-22.44
A3775	18.69	1.56	2.56	20.44	8.30	-22.44	-23.16	-23.61	0.51	0.61	0.20	0.04	-4.3	84.7	-22.63
A3781	22.30	7.13	6.10	—	—	-22.40	0.00	-22.40	—	0.56	0.05	0.24	72.8	39.8	-21.74
A3782	22.70	16.45	5.56	23.07	36.40	-23.75	-23.54	-24.41	1.22	0.70	0.08	0.37	-20.2	-52.9	-22.89
A3785	22.46	16.31	5.62	—	—	-24.07	0.00	-24.07	—	0.61	0.15	0.14	5.2	-13.3	-23.05
A3796	21.98	8.89	5.26	22.47	23.20	-23.19	-23.24	-23.97	0.95	0.65	0.22	0.32	-27.8	-43.8	-22.60
A3806	21.05	8.54	1.44	22.26	31.00	-23.36	-24.08	-24.53	0.52	0.90	0.14	0.21	67.4	62.2	-23.12

TABLE 2—*Continued*

Name (1)	$\mu_e$ (2)	$r_e$ (3)	$n$ (4)	$\mu_0$ (5)	$r_0$ (6)	$M_{Sersic}$ (7)	$M_{exp}$ (8)	$M_T$ (9)	$S/e$ (10)	$\alpha$ (11)	$e_{in}$ (12)	$e_{out}$ (13)	$pa_{in}$ (14)	$pa_{out}$ (15)	$M_{metric}$ (16)
A3809	26.22	144.88	7.30	—	—	-25.16	0.00	-25.16	—	0.81	0.13	0.44	87.0	88.9	-22.70
A3822	24.77	66.64	6.41	—	—	-24.87	0.00	-24.87	—	0.68	0.30	0.37	-22.8	-19.0	-22.87
A3825	17.26	0.61	4.05	20.68	4.40	-21.79	-21.26	-22.31	1.62	0.28	0.34	0.26	-46.8	-67.6	-21.53
A3826	22.59	26.06	3.19	—	—	-24.65	0.00	-24.65	—	0.81	0.35	0.38	-22.6	-23.0	-23.17
A3836	22.31	15.43	4.98	22.58	64.40	-24.16	-25.49	-25.77	0.29	0.80	0.15	0.43	-45.5	-23.7	-23.30
A3837	23.70	21.38	6.67	—	—	-23.56	0.00	-23.56	—	0.58	0.14	0.16	7.2	0.7	-22.45
A3844	20.25	2.77	4.37	24.30	56.02	-22.28	-23.32	-23.67	0.38	0.41	0.13	0.21	57.3	107.8	-21.75
A3851	20.01	3.52	1.16	20.95	11.90	-22.29	-23.23	-23.61	0.42	0.56	0.28	0.27	-88.6	78.1	-22.68
A3864	26.28	226.18	6.67	—	—	-26.15	0.00	-26.15	—	0.88	0.25	0.58	-45.9	-44.6	-23.18
A3869	21.94	10.51	6.41	—	—	-23.50	0.00	-23.50	—	0.45	0.19	0.27	-51.1	-52.5	-22.61
A3879	19.19	2.12	3.89	21.61	11.50	-22.67	-22.55	-23.36	1.13	0.56	0.23	0.25	-52.4	-37.5	-22.42
A3880	23.46	31.92	3.83	—	—	-24.24	0.00	-24.24	—	0.89	0.05	0.38	20.9	-37.4	-22.85
A3886	22.04	11.71	5.05	—	—	-23.69	0.00	-23.69	—	0.54	0.20	0.15	-2.7	5.1	-22.74
A3895	23.38	25.51	3.91	—	—	-23.85	0.00	-23.85	—	0.75	0.23	0.36	2.5	-6.2	-22.61
A3912	21.36	7.55	0.99	21.97	16.90	-22.57	-23.02	-23.57	0.66	0.91	0.17	0.26	34.8	15.8	-22.62
A3915	22.41	12.82	6.45	23.36	29.33	-23.74	-22.95	-24.17	2.08	0.71	0.17	0.29	86.9	87.3	-22.85
A3959	17.17	0.62	3.18	20.67	6.00	-21.92	-22.07	-22.75	0.87	0.46	0.42	0.45	22.6	20.3	-21.72
A3969	21.92	11.74	4.78	—	—	-24.00	0.00	-24.00	—	0.67	0.13	0.08	-24.5	-106.5	-23.02
A3985	23.46	38.82	3.07	—	—	-24.74	0.00	-24.74	—	0.92	0.44	0.61	30.5	30.4	-22.55
A4008	22.76	21.08	4.29	—	—	-24.10	0.00	-24.10	—	0.71	0.22	0.34	57.3	51.8	-22.91
A4038	23.76	31.17	7.41	—	—	-23.96	0.00	-23.96	—	0.57	0.15	0.36	-39.3	-47.1	-22.60
A4049	21.75	9.04	5.32	23.39	43.40	-23.26	-23.48	-24.12	0.81	0.57	0.08	0.12	66.6	47.8	-22.71
A4053	21.81	9.74	7.35	—	—	-23.63	0.00	-23.63	—	0.51	0.10	0.12	-85.0	-71.0	-22.71
A4059	24.17	77.05	4.41	—	—	-25.49	0.00	-25.49	—	0.98	0.22	0.41	-22.1	-23.2	-23.21

NOTE.—Col. (1), Abell Cluster; col (2), effective surface magnitude; col. (3), effective radius (kpc); col. (4),  $n$  parameter; col. (5), central surface magnitude; col. (6), scale length (kpc); col. (7), Sersic absolute magnitude; col. (8), exponential absolute magnitude; col. (9), total absolute magnitude; col. (10), Sérsic/exponential ratio; col. (11),  $\alpha$  parameter; col. (12), inner ellipticity; col. (13), outer ellipticity; col. (14), inner position angle ; col. (15), outer position angle; col. (16), Metric absolute magnitude.

TABLE 3  
BCGs PHOTOMETRICAL PARAMETERS (HOPKINS MODEL)

Name (1)	$\mu_e$ (2)	$r_e$ (3)	$n$ (4)	$\mu_0$ (5)	$r_0$ (6)	$M_{Sersic}$ (7)	$M_{exp}$ (8)	$M_T$ (9)	$e/S$ (10)
A0085	23.72	47.0	0.6	21.42	14.3	-23.91	-23.84	-24.63	0.935
A0133	23.23	39.0	1.2	21.04	6.9	-24.29	-22.66	-24.51	0.222
A0150	24.34	49.2	3.5	20.84	3.3	-24.22	-21.25	-24.29	0.065
A0152	22.77	20.5	1.4	19.63	1.7	-23.54	-21.07	-23.65	0.102
A0193	25.18	106.4	3.5	18.99	1.9	-25.04	-21.86	-25.10	0.053
A0194	22.05	14.2	1.7	18.39	1.1	-23.31	-21.09	-23.44	0.130
A0208	25.42	92.5	4.6	20.24	2.5	-24.87	-21.43	-24.91	0.042
A0257	22.64	18.5	1.9	19.72	2.1	-23.68	-21.58	-23.82	0.144
A0260	24.83	69.3	5.7	19.43	1.6	-24.66	-21.04	-24.70	0.036
A0262	23.41	34.9	1.8	20.07	2.4	-23.69	-20.92	-23.77	0.078
A0268	23.80	17.9	4.0	20.18	1.9	-22.77	-20.87	-22.95	0.173
A0279	24.02	52.5	3.1	20.46	3.3	-24.73	-21.70	-24.79	0.061
A0295	23.15	25.6	3.5	19.36	1.4	-23.95	-20.76	-24.01	0.053
A0311	25.52	146.2	3.6	20.73	3.6	-25.48	-21.57	-25.51	0.027
A0386	22.21	8.8	2.3	19.40	1.8	-22.54	-21.47	-22.88	0.375
A0397	23.88	37.9	2.9	19.39	2.0	-23.98	-21.50	-24.09	0.101
A0399	23.88	62.9	1.8	21.90	7.6	-24.97	-22.07	-25.05	0.069
A0404	23.08	21.0	1.5	20.35	3.7	-23.26	-22.01	-23.56	0.316
A0415	23.51	40.2	1.4	20.99	4.2	-24.88	-22.32	-24.98	0.095
A0498	25.12	73.3	3.8	20.83	2.6	-24.48	-20.85	-24.52	0.035
A0500	25.48	97.6	4.8	20.32	3.1	-24.91	-21.82	-24.97	0.058
A0539	24.12	39.2	3.8	19.37	1.7	-23.94	-21.24	-24.03	0.083
A0548	21.35	10.1	1.6	19.62	1.6	-23.32	-20.84	-23.42	0.102
A0553	24.88	65.0	4.5	20.60	3.2	-24.58	-21.57	-24.65	0.062
A0564	28.01	334.8	4.3	20.12	3.7	-25.03	-22.43	-25.13	0.091
A0564	27.66	267.4	4.0	20.12	3.7	-24.86	-22.43	-24.97	0.107
A0582	24.16	29.6	3.6	19.78	2.1	-23.45	-21.42	-23.61	0.154
A0671	23.68	51.2	2.9	19.72	3.1	-24.87	-22.19	-24.96	0.085
A0690	24.86	69.3	4.6	20.24	2.9	-24.74	-21.71	-24.80	0.062
A0757	23.71	19.1	3.4	20.67	2.9	-22.80	-21.10	-23.00	0.210
A0779	23.86	59.1	4.9	19.21	2.0	-24.89	-21.35	-24.93	0.038
A0780	23.55	37.2	3.1	19.28	1.6	-24.36	-21.22	-24.42	0.055
A0834	21.45	7.6	0.8	19.92	2.0	-22.39	-21.08	-22.68	0.299
A0841	24.10	44.4	3.3	19.95	2.8	-24.29	-21.86	-24.40	0.106
A0957	23.22	60.2	2.6	20.21	4.6	-24.69	-21.62	-24.75	0.059
A0970	26.34	97.5	6.1	20.98	2.5	-24.04	-20.52	-24.08	0.039
A0978	24.11	51.3	3.1	19.74	2.6	-24.50	-21.79	-24.58	0.083
A0979	24.11	36.7	5.0	20.74	2.2	-24.01	-20.50	-24.05	0.039
A0999	23.77	28.4	6.1	19.73	1.9	-23.71	-20.90	-23.79	0.075
A1003	22.78	20.3	1.5	19.45	1.7	-23.53	-21.26	-23.66	0.123
A1016	23.26	17.5	5.9	19.57	1.5	-23.16	-20.65	-23.26	0.099
A1020	23.68	24.5	3.9	20.14	2.5	-23.49	-21.40	-23.64	0.145
A1066	25.96	159.9	2.4	21.16	7.2	-25.05	-22.70	-25.17	0.115
A1069	22.80	26.3	2.0	20.06	2.4	-24.18	-21.37	-24.25	0.075
A1100	25.24	74.8	6.3	20.61	3.0	-24.52	-21.22	-24.57	0.048
A1139	24.75	52.6	5.3	19.76	1.7	-24.07	-20.79	-24.12	0.049
A1142	24.61	52.3	5.1	19.82	2.0	-24.12	-20.96	-24.18	0.055
A1149	24.61	49.6	5.0	18.58	1.3	-24.25	-21.61	-24.34	0.088
A1155	24.10	31.3	3.5	20.41	2.6	-23.61	-21.30	-23.73	0.120
A1171	25.40	70.1	3.6	21.09	4.3	-24.05	-21.66	-24.16	0.111
A1185	23.56	29.8	4.2	21.01	2.6	-23.86	-20.43	-23.91	0.042
A1187	22.87	22.1	1.9	20.08	3.0	-23.79	-21.93	-23.97	0.180
A1203	22.88	20.5	3.7	21.09	1.8	-23.94	-19.82	-23.97	0.022
A1216	22.89	15.7	3.5	19.78	1.8	-23.21	-21.00	-23.34	0.130
A1228	23.88	25.1	5.7	19.34	1.5	-23.34	-20.89	-23.45	0.105
A1238	25.50	92.3	4.0	20.11	2.3	-24.59	-21.24	-24.63	0.046
A1257	21.74	6.9	1.4	18.32	1.1	-21.96	-21.20	-22.40	0.495
A1308	25.48	70.4	6.5	21.05	2.6	-24.21	-20.55	-24.25	0.034



TABLE 3—*Continued*

Name (1)	$\mu_e$ (2)	$r_e$ (3)	$n$ (4)	$\mu_0$ (5)	$r_0$ (6)	$M_{Sersic}$ (7)	$M_{exp}$ (8)	$M_T$ (9)	$e/S$ (10)
A1314	24.79	77.1	4.0	19.18	2.2	-24.66	-21.86	-24.73	0.076
A1317	25.12	137.6	2.4	20.74	4.8	-25.57	-22.23	-25.62	0.046
A1424	21.93	14.6	1.7	19.19	1.9	-23.77	-21.87	-23.95	0.172
A1474	21.45	12.3	1.0	19.65	1.6	-23.68	-21.09	-23.78	0.092
A1507	22.83	22.4	1.5	19.88	2.7	-23.68	-21.86	-23.87	0.187
A1520	24.64	85.8	4.2	19.94	2.8	-25.31	-21.86	-25.36	0.042
A1534	24.13	41.4	5.5	20.55	3.1	-24.41	-21.50	-24.48	0.069
A1569	21.95	17.1	1.5	19.36	2.0	-24.04	-21.76	-24.17	0.122
A1610	24.34	42.5	7.3	19.86	1.8	-24.36	-20.91	-24.41	0.042
A1648	23.72	43.6	1.0	20.55	5.2	-24.06	-22.62	-24.32	0.266
A1749	23.59	35.7	3.6	19.78	2.9	-24.34	-22.07	-24.46	0.124
A1773	23.91	47.2	2.3	20.27	3.4	-24.47	-22.00	-24.58	0.102
A1775	23.22	31.5	1.5	20.76	5.3	-24.04	-22.42	-24.26	0.224
A1795	27.15	354.7	6.2	20.98	3.5	-26.09	-21.33	-26.11	0.012
A1809	24.65	76.6	3.8	20.12	3.5	-25.03	-22.16	-25.11	0.071
A1831	23.96	63.7	3.0	20.23	2.7	-25.23	-21.54	-25.27	0.033
A1904	23.73	45.6	3.6	19.97	2.3	-24.82	-21.43	-24.86	0.044
A1964	24.18	44.1	2.1	20.01	2.8	-23.97	-21.75	-24.10	0.130
A1982	22.43	19.8	1.0	19.98	3.2	-23.56	-22.08	-23.81	0.255
A2022	24.80	65.6	3.7	19.72	2.5	-24.45	-21.81	-24.54	0.088
A2028	25.46	100.1	6.2	21.10	3.8	-25.06	-21.37	-25.09	0.033
A2040	27.66	561.3	5.0	19.87	2.2	-26.34	-21.29	-26.35	0.010
A2147	28.07	691.6	5.8	21.17	5.5	-26.45	-21.97	-26.47	0.016
A2151	22.94	25.4	2.1	19.55	1.9	-23.77	-21.20	-23.87	0.093
A2162	23.02	26.1	3.8	19.33	1.9	-24.02	-21.31	-24.11	0.083
A2197	22.23	23.8	2.6	19.21	2.6	-24.37	-22.11	-24.50	0.125
A2199	24.12	58.2	2.9	21.38	5.6	-24.50	-21.64	-24.57	0.072
A2309	23.92	31.3	4.0	19.46	1.9	-23.72	-21.39	-23.84	0.117
A2319	22.72	31.0	1.7	20.71	1.9	-24.58	-20.22	-24.60	0.018
A2331	24.38	51.1	3.2	20.32	1.8	-24.35	-20.52	-24.38	0.029
A2366	23.62	35.0	3.0	19.58	2.8	-24.14	-22.15	-24.30	0.160
A2372	25.34	64.3	7.2	20.68	3.7	-24.22	-21.67	-24.32	0.095
A2457	24.65	71.8	4.8	20.76	3.8	-24.93	-21.66	-24.98	0.049
A2462	25.41	86.2	4.6	19.83	2.6	-24.71	-21.90	-24.79	0.075
A2480	26.55	144.4	7.5	19.60	2.2	-24.92	-21.73	-24.98	0.053
A2492	23.84	30.6	4.1	20.70	2.8	-23.95	-21.19	-24.03	0.079
A2524	23.20	25.6	2.3	20.34	2.9	-23.95	-21.68	-24.07	0.124
A2559	23.14	41.4	2.2	20.31	2.5	-24.92	-21.29	-24.96	0.035
A2572	28.80	602.5	9.1	19.36	2.2	-25.67	-21.82	-25.70	0.029
A2572	26.02	131.5	5.2	19.25	2.3	-24.84	-21.95	-24.91	0.070
A2593	22.92	19.5	1.4	20.52	1.7	-23.22	-20.17	-23.28	0.060
A2626	22.92	29.0	2.3	19.18	0.8	-24.40	-19.93	-24.41	0.016
A2634	26.93	283.2	7.8	19.56	1.7	-25.77	-21.01	-25.78	0.012
A2656	23.03	22.8	2.0	19.69	1.7	-23.77	-21.19	-23.87	0.093
A2657	21.19	5.5	1.4	17.45	0.5	-22.11	-20.30	-22.29	0.190
A2660	25.01	64.9	6.5	20.11	1.7	-24.49	-20.51	-24.52	0.026
A2670	23.54	40.8	2.6	19.84	2.8	-24.57	-21.99	-24.67	0.092
A2717	23.39	36.5	1.8	19.73	2.0	-24.16	-21.29	-24.24	0.071
A2734	25.48	127.8	3.9	22.45	8.1	-25.27	-21.62	-25.30	0.035
A2806	21.68	9.0	1.4	19.09	1.8	-22.64	-21.51	-22.96	0.355
A2841	23.70	35.1	4.1	19.77	2.2	-24.28	-21.48	-24.36	0.076
A2859	23.75	25.0	3.6	20.30	2.4	-23.42	-21.13	-23.54	0.122
A2864	23.50	18.1	3.2	19.73	1.6	-22.93	-20.92	-23.08	0.158
A2877	22.94	37.7	4.1	18.62	1.8	-24.78	-21.80	-24.85	0.064
A2881	23.03	12.8	3.7	19.62	1.6	-22.70	-20.92	-22.89	0.195
A2896	21.99	11.1	3.5	18.84	1.4	-23.15	-21.16	-23.31	0.159
A3045	23.17	17.9	1.0	20.47	3.7	-22.68	-21.95	-23.13	0.508
A3095	22.61	15.0	1.3	19.73	2.6	-22.94	-21.91	-23.30	0.389

TABLE 3—*Continued*

Name (1)	$\mu_e$ (2)	$r_e$ (3)	$n$ (4)	$\mu_0$ (5)	$r_0$ (6)	$M_{Sersic}$ (7)	$M_{exp}$ (8)	$M_T$ (9)	$e/S$ (10)
A3104	23.26	36.3	1.3	19.82	2.7	-24.25	-21.94	-24.37	0.119
A3107	25.84	75.1	4.5	20.61	2.9	-23.85	-21.24	-23.94	0.091
A3110	22.02	18.5	0.9	19.93	5.0	-23.84	-23.13	-24.30	0.518
A3111	23.57	33.6	2.9	20.66	2.7	-24.18	-21.07	-24.24	0.057
A3112	23.91	74.2	2.5	21.08	4.2	-25.48	-21.62	-25.51	0.028
A3120	24.82	74.4	3.9	20.58	2.8	-24.64	-21.07	-24.68	0.037
A3122	24.29	44.8	6.0	19.48	2.3	-24.43	-21.85	-24.53	0.093
A3123	21.98	11.5	1.3	18.95	1.7	-22.97	-21.74	-23.27	0.322
A3125	22.59	11.8	0.9	19.85	2.6	-22.25	-21.74	-22.78	0.625
A3142	24.48	47.9	4.8	20.69	2.7	-24.26	-21.05	-24.32	0.052
A3223	23.05	23.3	2.8	20.35	3.5	-23.83	-21.86	-23.99	0.164
A3225	22.16	12.9	1.1	19.58	2.3	-22.93	-21.75	-23.24	0.337
A3266	22.83	43.6	1.3	19.92	3.1	-25.01	-22.04	-25.08	0.064
A3301	26.53	240.0	5.2	20.89	5.2	-25.70	-22.20	-25.74	0.040
A3332	28.15	326.5	9.2	20.84	3.7	-25.16	-21.63	-25.20	0.039
A3336	24.45	61.0	2.8	21.20	5.0	-24.60	-21.89	-24.69	0.082
A3341	24.76	57.7	4.5	19.29	1.4	-24.22	-20.80	-24.26	0.043
A3354	26.09	80.0	6.8	20.56	3.4	-23.93	-21.63	-24.05	0.121
A3374	20.79	6.5	1.0	17.99	0.6	-22.72	-20.43	-22.85	0.121
A3376	25.10	85.9	5.2	20.43	3.3	-24.89	-21.63	-24.95	0.050
A3380	28.80	593.9	7.4	20.62	3.3	-25.57	-21.44	-25.60	0.022
A3390	24.31	39.8	4.2	19.74	1.6	-23.84	-20.68	-23.89	0.055
A3408	25.06	82.1	5.1	20.16	2.8	-24.78	-21.52	-24.84	0.049
A3420	23.56	19.3	2.8	20.43	2.7	-22.91	-21.29	-23.13	0.224
A3528	24.78	92.0	3.8	19.92	2.7	-25.30	-21.83	-25.34	0.041
A3530	24.04	67.3	3.2	19.93	2.1	-25.25	-21.28	-25.28	0.026
A3531	24.96	56.2	3.2	19.73	1.2	-23.85	-20.09	-23.88	0.031
A3532	28.22	728.6	6.5	20.37	2.8	-26.64	-21.44	-26.65	0.008
A3554	23.45	41.2	2.5	19.18	1.3	-24.60	-20.96	-24.64	0.035
A3559	22.75	29.3	2.0	18.85	1.9	-24.45	-22.08	-24.56	0.113
A3562	28.77	1160.1	6.9	21.30	5.1	-27.08	-21.77	-27.09	0.007
A3574	23.36	48.2	3.3	18.52	1.0	-24.53	-20.40	-24.55	0.022
A3605	27.28	305.7	4.1	21.47	8.2	-25.42	-22.67	-25.51	0.079
A3667	28.77	812.0	8.6	21.39	5.8	-26.37	-21.91	-26.39	0.016
A3703	25.45	101.2	3.6	21.19	4.3	-24.78	-21.54	-24.83	0.051
A3716	23.49	40.6	2.6	19.79	2.1	-24.49	-21.31	-24.55	0.053
A3731	25.84	94.8	7.1	20.15	2.7	-24.53	-21.47	-24.59	0.060
A3733	23.48	24.2	1.9	20.17	2.3	-23.18	-21.08	-23.33	0.144
A3741	25.47	86.1	3.4	21.18	3.9	-24.40	-21.35	-24.47	0.060
A3782	26.04	130.0	6.8	20.76	2.7	-25.02	-20.88	-25.04	0.022
A3796	24.66	54.6	3.6	20.77	3.1	-24.25	-21.24	-24.32	0.062
A3806	25.01	81.3	4.9	21.63	6.7	-24.93	-22.09	-25.01	0.073
A3825	22.15	6.8	0.7	19.41	1.5	-21.23	-20.85	-21.81	0.699
A3844	26.38	66.8	3.7	20.79	3.0	-22.96	-21.15	-23.15	0.188
A3851	22.90	21.1	1.9	20.12	3.1	-23.54	-21.83	-23.75	0.206
A3879	23.17	18.3	3.1	19.24	1.7	-23.26	-21.49	-23.45	0.196
A3897	24.94	67.7	3.8	19.84	2.6	-24.55	-21.88	-24.64	0.085
A3912	23.93	30.6	1.4	21.46	7.6	-23.20	-22.49	-23.65	0.518
A4049	23.85	31.5	4.4	19.63	1.8	-23.77	-21.03	-23.86	0.080

NOTE.—Col. (1), Abell Cluster; col. (2), effective surface magnitude; col. (3), effective radius (kpc); col. (4),  $n$  parameter; col. (5), central surface magnitude; col. (6), scale length (kpc); col. (7), Sersic absolute magnitude; col. (8), exponential absolute magnitude; col. (9), total absolute magnitude; col. (10), exponential/Sérsic ratio.